CHALMERS

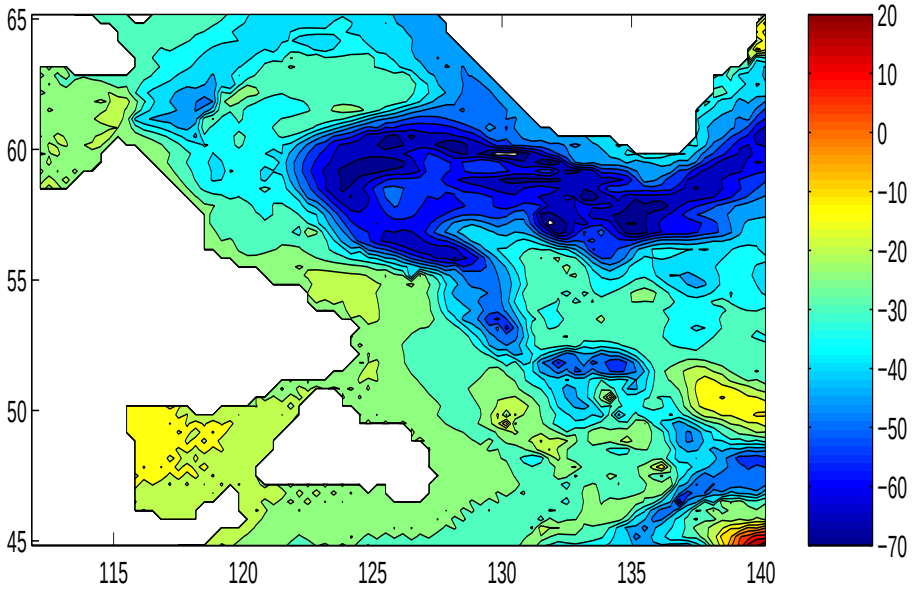

An Examination of the Labrador Sea in the Winters of 2002-2004 using ARGO floats

Ting On Chan

Department of Earth and Atmospheric Science
UNIVERSITY OF ALBERTA
Edmonton, Canada

Department of Water Environment Transport
CHALMERS UNIVERSITY OF TECHNOLOGY
Göteborg, Sweden

†The above figure shows the sea surface height(cm) of the Labrador Sea from a model of the North Atlantic, representing May, 2004

Abstract

The deep convection in the Labrador Sea during winters plays an important role in stabilizing the global climate systems in terms of the global thermohaline circulation. The winters of 2002-2004 in the Labrador Sea are investigated using Argo floats and an eddy-permitting model of the sub-polar North Atlantic. The hydrographic data of the Labrador Sea have been difficult to collect due to tough winter conditions and therefore scarce until recent advent of autonomous floats. More recently, the establishment of Argo (Array for Real-time Geostrophic Oceanography) started a new era for the worldwide measurement and access of the hydrographic data in near real-time. In this paper, the intermediate depth (1000 m - 2000 m) is focused. Important oceanic quantities such as mixed layer depths (MLD), Labrador Sea Water (LSW) distributions and trajectories of the floats are studied. The analogies and deviations between the observational and modelling results are discussed.

Both the observational and modelling results suggest that there are little or no convection during 2002 - 2004. Among these three years, both the results of 2003 show the strongest deep convection ($\sim$1100 m). The observational convection are found around the western and central Labrador Sea region while the modelling convection mainly distribute along the southern coast of Cape Farewell and eastern Labrador Sea. The trajectories from the float data depict reasonable circulation paths, especially in 2003: the Deep Western Boundary Current (DWBC) is presented. The overall results demonstrate successfully the high annual variability of the Labrador Sea in winters.

KEYWORDS: Labrador Sea, Argo, deep convection.

Sammanfattning

Djupomblandningen i Labradorhavet utgör en viktig länk i den globala termohalina cirkulationen, vilken i sin tur spelar en avgörande roll i det globala klimatsystemet. Vintrarna 2002-2004 har djupomblandningen i Labradorhavet studerats med hjälp av mätningar med 'Argobojar' (Argo floats) och en hydrodynamisk numerisk modell över den subpolara delen av Nordatlanten. Modellen kan modellera virvlar. Det har tidigare varit svårt att samla in hydrografiska data från Labradorhavet på grund av stränga vinterförhållanden, men med nya autonoma bojar är det numera enklare. Med upprättandet av Argo (Array for Real-time Geostrophic Oceanography) startade en ny era av världsomfattande observationer tillgängliga i nästan realtid. Detta examensarbete fokuserar påintermediärt djupvatten (1000 m - 2000 m). Viktiga oceanografiska kvantiteter som omblandningslagrets mäktighet (Mixed layer depth, MLD), fördelningen av Labradorhavsvatten (LSW), och bojarnas rörelser har studerats. Likheter och olikheter mellan observationer och modellering diskuteras.

Både observationerna och modelleringsresultaten antyder att djupomblandningen var obetydlig under åren 2002 till 2004. Av de tre åren uppvisar år 2003 den kraftigaste djupomblandningen, cirka 1100 m. Den observerade djupomblandningen uppträder i västra och centrala Labradorhavet, medan enligt modellen den omblandningen mest uppträder längs Grönlands sydkust vid Kap Farväl och i östra Labradorhavet. Spårlinjerna efter bojarna ger ett rimligt cirkulationsmönster år 2003 och återger också den djupa västra gränsströmmen (Deep Western Boundary Current, DWBC). Allmänt lyckas resultaten återge den årliga stora variationen mellan vintrarna i Labradorhavet.

Nyckelord: Labradorhavet, Argo, Djupomblandningen

Preface

This paper is based on a half year study from June 2004 to November 2004 in the Geophysical Fluid Dynamics Modelling Labratory of the Department of Earth and Atmospheric Science, the University of Alberta, and this is submitted as a master thesis to Chalmers University of Technology for the Master of Science in Applied Environmental Measurement Techniques (AEMT). This work is funded by a Canadian Foundation for Climate and Atmospheric Sciences grant awarded to Dr. Paul Myers.

Argo was newly established in 2000 and it aimed at maintaining a global ocean monitoring network which can collect oceanic data continuously in real time. The Labrador Sea is a sea heavily studied in recent years and represents a crucial area for the global ocean circulation and the global climate system. Labrador Sea data have long been difficult to collect in winters due to severe conditions. Now with autonomous Argo floats, the Labrador Sea and other oceans can be studied more intensively and provides the motivation behind this work.

Acknowledgments

I would like to express special thanks to my supervisor, Dr. Paul Myers for his guidance and patience throughout the thesis work, as well as for bringing me into the big world of physical oceanography. Also I give thanks to his research group especially Dr. Sven Harig, Michelle Li, Duo Yang, Nilgun Cetin, Brett Wheler, for their assistance and sharing.

I am grateful to Dr. Cynthia Yau, who guided me into the fields of environmental science and oceanography with a lot of encouragement.

For Chalmers University of Technology, I would like to thank Dr. Ann-Margret Strömvall who gave excellent AEMT courses, also Professor Lars Bergdahl for being my thesis examiner and translating the abstract to Swedish and also Dr. Göran Björk (Department of Oceanography, Göteborg University) for joining the examination of my thesis, Oskar Modin and Bharath Srinivasan for being my reviewers.

Thanks also go to a long list of those who did not know me for long time, but helped me a lot during my stay in Sweden and Canada.

Last but not least, I thank my dearest dad, Mr. Wing Wah Chan and my mom Mrs. Sui Heung Ng Chan for their endless love, as well as my two lovely sisters Wing Yee and Pui Yi, for their wisdom and encouragement.

Edmonton, January 10, 2005

TING ON CHAN

CONTENTS

1 INTRODUCTION **1**

1.1 Labrador Sea 1

1.2 Surface and deep circulation in the Labrador Sea 1

1.3 Deep Convection 2

1.4 Labrador Sea Water Formation and Dispersal 4

1.4.1 Mixed layer depths 4

1.4.2 Spreading of the LSW 5

1.5 Measurement techniques and international program in physical oceanography 5

1.5.1 Basic principle 5

1.5.2 ARGO 6

1.6 Introduction to oceanic general circulation model 6

1.7 The aims and the organization of the paper 8

2 Interannual study of the Labrador Sea **10**

2.1 Data Set 10

2.2 Potential temperature, salinity and potential density 10

2.2.1 Potential temperature distribution at 1000 m, 1500 m, 2000 m . . 10

2.2.2 Salinity distribution at 1000 m, 1500 m, 2000 m 13

2.2.3 Potential density distribution at 1000 m, 1500 m, 2000 m 18

2.2.4 Average values in 55N - 65N, 55N - 65N, 50N - 60N and 45N - 65N 20

2.3 Mixed layer depth 22

2.4 Heat content 26

2.5 Trajectories of the floats at 2000 m 32

2.6 Energy 32
2.7 LSW thickness and the depth of potential vorticity 34

3 Ocean Modelling **37**

3.1 Sub-polar Ocean Model 37
3.2 Model forcing fields 38
3.3 Model results 41
3.3.1 Mixed Layer Depth 41
3.3.2 Heat content 43
3.3.3 Circulation 43
3.3.4 Energy 44

4 Conclusion and Discussion **50**

List of Figures

1.1 The surface currents in Labrador Sea (Lazier *et. al* 2002) 2

1.2 A simplified schematic diagram of the three phases of open ocean deep convection: (a) ocean cross section, (b) cyclonic condition , (c) atmospheric forcing (d) deep sinking (e) lateral exchange (f) spreading. 3

2.1 The potential temperature, θ at 1000 m in Labrador Sea. $\theta \leq 3^o$ C is marked green circles, $3 < \theta \leq 3.2^o$ C with blue squares, $3.2 < \theta \leq 3.4^o$ C with light blue triangles, $3.4 < \theta \leq 3.6^o$ C with red diamonds, $3.6 < \theta \leq 3.8^o$ C with yellow pentagons, and $\theta > 3.8^o$ C with purple hexagons 11

2.2 The potential temperature, θ at 1500 m in Labrador Sea. $\theta \leq 3^o$ C is marked green circles, $3 < \theta \leq 3.2^o$ C with blue squares, $3.2 < \theta \leq 3.4^o$ C with light blue triangles, $3.4 < \theta \leq 3.6^o$ C with red diamonds, $3.6 < \theta \leq 3.8^o$ C with yellow pentagons, and $\theta > 3.8^o$ C with purple hexagons 11

2.3 The potential temperature, θ at 2000 m in Labrador Sea. $\theta \leq 3^o$ C is marked with green circles, $3 < \theta \leq 3.2^o$ C with blue squares, $3.2 < \theta \leq 3.4^o$ C with light blue triangles, $3.4 < \theta \leq 3.6^o$ C with red diamonds, $3.6 < \theta \leq 3.8^o$ C with yellow pentagons, and $\theta > 3.8^o$ C with purple hexagons 12

2.4 The salinity, s at 1000 m in Labrador Sea. $s \leq 34.8$ psu is marked with green circles, $34.8 < s \leq 34.84$ psu with blue squares, $3.84 < s \leq 34.88$ psu with light blue triangles, $34.88 < s \leq 34.92$ psu with red diamonds, $34.92 < s \leq 35$ psu with yellow pentagons, and $s > 35$ psu with purple hexagons 13

2.5 The salinity, s at 1500 m in Labrador Sea. $s \leq 34.8$ psu is marked with green circles, $34.8 < s \leq 34.84$ psu with blue squares, $3.84 < s \leq 34.88$ psu with light blue triangles, $34.88 < s \leq 34.92$ psu with red diamonds, $34.92 < s \leq 35$ psu with yellow pentagons, and $s > 35$ psu with purple hexagons 14

2.6 The salinity, s at 2000 m in Labrador Sea. $s \leq 34.8$ psu is marked with green circles, $34.8 < s \leq 34.84$ psu with blue squares, $3.84 < s \leq 34.88$ psu with light blue triangles, $34.88 < s \leq 34.92$ psu with red diamonds, $34.92 < s \leq 35$ psu with yellow pentagons, and $s > 35$ psu with purple hexagons 14

2.7 The potential density, σ_θ at 1000 m in Labrador Sea. $\sigma_\theta \leq 27.65$ kgm^{-3} is marked with green circles, $27.65 < \sigma_\theta \leq 27.7$ kgm^{-3} with blue squares, $27.7 < \sigma_\theta \leq 27.74$ kgm^{-3}with light blue triangles, $27.74 < \sigma_\theta \leq 27.76$ kgm^{-3} with red diamonds, $27.76 < \sigma_\theta \leq 27.78$ kgm^{-3} with yellow pentagons, $27.78 < \sigma_\theta \leq 27.8$ kgm^{-3} with black cross, and $\sigma_\theta > 27.8$ kgm^{-3} with purple hexagons 15

2.8 The potential density, σ_θ at 1500 m in Labrador Sea. $\sigma_\theta \leq 27.7$ kgm^{-3} is marked with green circles, $27.7 < \sigma_\theta \leq 27.72$ kgm^{-3} with blue squares, $27.72 < \sigma_\theta \leq 27.74$ kgm^{-3}with light blue triangles, $27.74 < \sigma_\theta \leq 27.76$ kgm^{-3} with red diamonds, $27.76 < \sigma_\theta \leq 27.78$ kgm^{-3} with yellow pentagons, $27.78 < \sigma_\theta \leq 27.8$ kgm^{-3} with black cross, and $\sigma_\theta > 27.8$ kgm^{-3} with purple hexagons 16

2.9 The potential density, σ_θ at 2000 m in Labrador Sea. $\sigma_\theta \leq 27.7$ kgm^{-3} is marked with green circles, $27.7 < \sigma_\theta \leq 27.72$ kgm^{-3} with blue squares, $27.72 < \sigma_\theta \leq 27.74$ kgm^{-3}with light blue triangles, $27.74 < \sigma_\theta \leq 27.76$ kgm^{-3} with red diamonds, $27.76 < \sigma_\theta \leq 27.78$ kgm^{-3} with yellow pentagons, $27.78 < \sigma_\theta \leq 27.8$ kgm^{-3} with black cross, and $\sigma_\theta > 27.8$ kgm^{-3} with purple hexagons 17

2.10 Spreading paths of LSW (σ_θ between 27.74 and 27.8) at 1500m in 2003 long winter: green circles denote profiles in November, light blue triangles denote profiles in December, blue squares denote profiles in January, red diamonds denote profiles in February, yellow pentagons denotes profiles in March, black crosses denotes profiles in April and purple hexagons denote profiles in May . . 18

2.11 Spreading paths of LSW (σ_θ between 27.74 and 27.8) at 1500m in 2004 long winter: green circles denote profiles in November, light blue triangles denote profiles in December, blue squares denote profiles in January, red diamonds denote profiles in February, yellow pentagons denotes profiles in March, black crosses denotes profiles in April and purple hexagons denote profiles in May . . 19

2.12 The average θ vs depth in different regions of Labrador Sea (Latitude range), unit: ^{o}C, a filled line denotes 2002, a dash line denotes 2003, a dotted line denotes 2004. 20

2.13 The average salinity vs depth in different regions of Labrador Sea (Latitude range), unit: psu, a filled line denotes 2002, a dash line denotes 2003, a dotted line denotes 2004. 21

2.14 The average σ_θ vs depth in different regions of Labrador Sea (Latitude range, unit: kgm^{-3}, a filled line denotes 2002, a dash line denotes 2003, dotted line denotes 2004. 21

2.15 The mixed layer depth, MLD in Labrador Sea. MLD $\leq$ 200 m is marked with green circles, 200 $<$ MLD $\leq$ 500 m with blue squares, 500 $<$ MLD $\leq$ 800 m with light purple triangles, 800 m $<$ MLD $\leq$ 1100 m with red diamonds, 1100 m $<$ MLD $\leq$ 1600 m with black pentagons, and MLD $>$ 1600 m with purple hexagons 23

2.16 The monthly average (January to March) of wind stress and sea surface temperature. 24

2.17 Time Series of MLDs from 2002-2004 with 0.03 kgm^{-3} density criterion, red crosses emphasise MLD $>$ 800 m 25

2.18 The heat content, HC above 1000 m, 1300 m, and 1600 m in the short winter (Jan - March winter). $0 < HC \leq 1 \times 10^{10}$ Jm^{-2} is marked with blue squares, $1 \times 10^{10} < HC \leq 2 \times 10^{10}$ Jm^{-2} with light blue triangles, $2 \times 10^{10} < HC \leq 3 \times 10^{10}$ Jm^{-2} with red diamonds, $3 \times 10^{10} < HC \leq 4 \times 10^{10}$ Jm^{-2} with yellow pentagons, and $HC > 4 \times 10^{10}$ Jm^{-2} with purple hexagons 27

2.19 The heat content, HC above 1000 m, 1300 m, and 1600 m in the long winter (November -May winter). $0 < HC \leq 1 \times 10^{10}$ Jm^{-2} is marked with blue squares, $1 \times 10^{10} < HC \leq 2 \times 10^{10}$ Jm^{-2} with light blue triangles, $2 \times 10^{10} < HC \leq 3 \times 10^{10}$ Jm^{-2} with red diamonds, $3 \times 10^{10} < HC \leq 4 \times 10^{10}$ Jm^{-2} with yellow pentagons, and $HC > 4 \times 10^{10}$ Jm^{-2} with purple hexagons 28

2.20 Trajectories of 7 floats at 2000 m in 2002 long (November-May) winter, squares denote the deployment locations of the floats 29

2.21 Trajectories of 19 floats at 2000 m in 2003 long (November-May) winter, squares denote the deployment locations of the floats 30

2.22 Trajectories of 23 floats at 2000 m in 2004 long (November-May) winter, squares denote the deployment locations of the floats 31

2.23 MKE, EKE, velocity derived from EKE for 2002-2004 long winters. The unit of MKE and EKE is cm^{2}s^{-2}, and the unit of velocity, v is cms^{-1} 33

2.24 The thickness of the Labrador Sea Water, t is shown. $t \leq 600$ m is marked with green circles, $600 < t \leq 700$ m with blue squares, $700 < t \leq 800$ m with light blue triangles, $800 < t \leq 900$ m with red diamonds, $900 < t \leq 1000$ m with yellow pentagons, and $t > 1000$ m with purple hexagons 34

2.25 The depth of the potential vorticity minimum , d is shown. $d \leq 500$ m is marked with green circles, $500 < d \leq 750$ m with blue squares, $750 < d \leq 1000$ m with light blue triangles, $1000 < d \leq 1250$ m with red diamonds, $1250 < d \leq 1500$ m with yellow pentagons, and $d > 1500$ m with purple hexagons 35

3.1 Monthly-averaged wind stress applied to the model for January 39

3.2 Monthly-averaged wind stress applied to the model for July 39

3.3 Sea surface temperature applied to the model for January 40

3.4 Sea surface temperature applied to the model for July 40

3.5 Model mixed layer depth, MLD. MLD $\leq$ 200 m is marked green circles, 200 $<$ MLD $\leq$ 500 m with blue squares, 500 $<$ MLD $\leq$ 800 m with light purple triangles, 800 m $<$ MLD $\leq$ 1100 m with red diamonds, 1100 m $<$ MLD $\leq$ 1600 m with black pentagons, and MLD $>$ 1600 m with purple hexagons . . . 41

3.6 Model mixed layer depth with additional content in the central Labrador Sea in 2002, MLD. MLD $\leq$ 200 m is marked with green circles, 200 $<$ MLD $\leq$ 500 m with blue squares, 500 $<$ MLD $\leq$ 800 m with light purple triangles, 800 m $<$ MLD $\leq$ 1100 m with red diamonds, 1100 m $<$ MLD $\leq$ 1600 m with black pentagons, and MLD $>$ 1600 m with purple hexagons 42

3.7 Model Heat Content in short (Jan-Mar) winter. $0 < HC \leq 1 \times 10^{10}$ Jm^{-2} is marked with blue squares, $1 \times 10^{10} < HC \leq 2 \times 10^{10}$ Jm^{-2} with light blue triangles, $2 \times 10^{10} < HC \leq 3 \times 10^{10}$ Jm^{-2} with red diamonds, $3 \times 10^{10} < HC \leq 4 \times 10^{10}$ Jm^{-2} with yellow pentagons, and $HC > 4 \times 10^{10}$ Jm^{-2} with purple hexagons 43

3.8 Model Heat Content in long (Nov-May) winter. $0 < HC \leq 1 \times 10^{10}$ Jm^{-2} is marked with blue squares, $1 \times 10^{10} < HC \leq 2 \times 10^{10}$ Jm^{-2} with light blue triangles, $2 \times 10^{10} < HC \leq 3 \times 10^{10}$ Jm^{-2} with red diamonds, $3 \times 10^{10} < HC \leq 4 \times 10^{10}$ Jm^{-2} with yellow pentagons, and $HC > 4 \times 10^{10}$ Jm^{-2} with purple hexagons 44

3.9 Average currents on the depth 1930 m during the 2002 long winter (22nd model level of Myers (2002b)) 45

3.10 Average currents on the depth 1930 m during the 2003 long winter (22nd model level of Myers (2002b)) 46

3.11 Average currents on the depth 1930 m during the 2004 long winter (22nd model level of Myers (2002b)) 47

3.12 Model MKE, EKE, velocity derived from EKE for 2002-2004 long winters. The unit of MKE and EKE is cm^{2}s^{-2}, and the unit of velocity, v is cms^{-1} . . . 48

List of Tables

2.1 Mixed layer depth statistic 23

2.2 Average MLD in different regions, unit (m) 26

3.1 SPOM parameters and features 37

1 INTRODUCTION

1.1 Labrador Sea

The Labrador Sea is located between northeast Canada and southern Greenland. Together with the Greenland and Mediterranean Seas, it is one of the locations of open ocean deep convection in the Northern Hemisphere (Marshall and Schott 1999). During winters, extremely cold winds with an average temperature colder than -30^o C and average speeds of 6 ms^{-1} chill the upper ocean causing deep convection which produces the intermediate-depth water mass known as Labrador Sea Water (LSW). LSW is one of the components of North Atlantic Deep Water (NADW) and it is characterized with low temperature, low salinity and a minimum potential vorticity with a core density between the isopycnals of 27.74 and 27.8 kgm^{-3} (Stramma *et al.* 2004). It spreads throughout the North Atlantic Ocean through three main pathways (Talley and McCartney 1982) and contributes to the sub-polar circulation and the global thermohaline circulation, and thus may interact with the global climate (Dickson 1997).

1.2 Surface and deep circulation in the Labrador Sea

Both the surface and deep circulations in the Labrador Sea are generally cyclonic (Clarke and Gascard 1983). Figure 1.1 shows the Labrador Sea bounded by the West Greenland Current (WGC) and the Labrador Current (LC), and in the northwest corner (52^oN) region flows the North Atlantic Current (NAC). East Greenland Current (EGC) flows along the east coast of Greenland from Fram Strait to Cape Farewell and transports water from the the Arctic and the Nordic Seas to the North Atlantic with annual mean transport 21$\pm$3 Sv (Sverdrup (Sv); 1 Sv = 10^6 m^3s^{-1})(Woodgate *et al.* 1999). Its maximum speed in the upper 500 m can reach 20 - 30 cms^{-1} (Bersch 1995). After EGC has flowed past Cape Farewell, at the southern tip of Greenland, its contination, the West Greenland Current flows northward along the west coast of Greenland and transport approximately 3 Sv of fresh and cold water. Eulerian measured speed of the shallow WGC is 35 cms^{-1} while Lagrangian measured speed along the 2000 m isobath reach 95 cms^{-1} (Cuny *et al.* 2001). The WGC divides into two branches roughly at 63^oN; one of them continues flowing northward along the west coast of Greenland, while the other one southwestward and converges into the Labrador Current (Cuny *et al.* 2001). The LC flows from Hudson Strait to the Tail of Grand Banks of Newfoundland and transports a mixture of the cold and fresh water brought by the Baffin Island Current flowing out from Baffin Bay, and warmer and more saline water brought by the WGC and its offshore component, the Irminger Current (IC). As with the WGC does, the LC

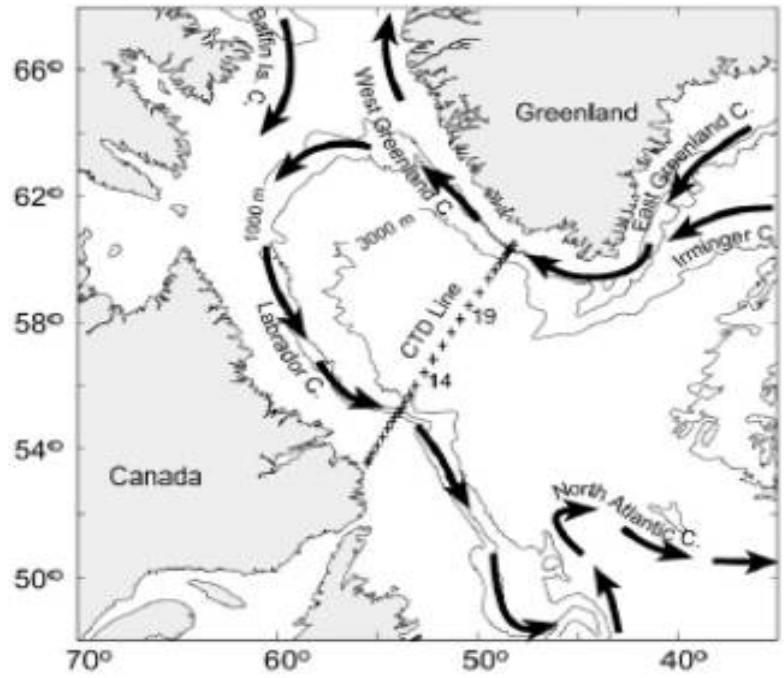

Figure 1.1. The surface currents in Labrador Sea (Lazier *et. al* 2002)

produces two branches around Hamilton Bank, with the offshore branch, transporting 85 % of total water with average speeds of around 5 - 10 cms^{-1} and maximum speed of 36 ± 16 cms^{-1} (Lazier and Wright 1993). For the deep circulation, the Deep Western Boundary Current (DWBC) carries North Atlantic Deep Water (NADW) which contains LSW, at depths of 700 m - 4000 m and flows equatorward along the western boundary of the Atlantic.

1.3 Deep Convection

Deep sea convection is basically a deep vertical overturn triggered by a large buoyancy loss at the sea surface, with a homogenous vertical water column (water masses) produced. The thickness of this homogenous water column is known as the mixed layer depth (MLD). The essential conditions for deep convection to occur are: strong atmospheric forcing, weak stratification in the upper ocean and the underlying water which can upwell to the surface readily (LabSeaGroup 1998). Three phases for the deep convection are identified, referring to figure 1.2. The first phase is the preconditioning. At the beginning, the ocean is stratified with density generally increasing with depths (figure 1.2(a)). The cyclonic circulation brings the weakly stratified water (figure 1.2(b)) in the interior close to the surface for heat exchange with the atmosphere on the large-scale (order of 100 km). The second stage is the deep convection. The surface water becomes dense once it loses its heat and buoyancy (figure

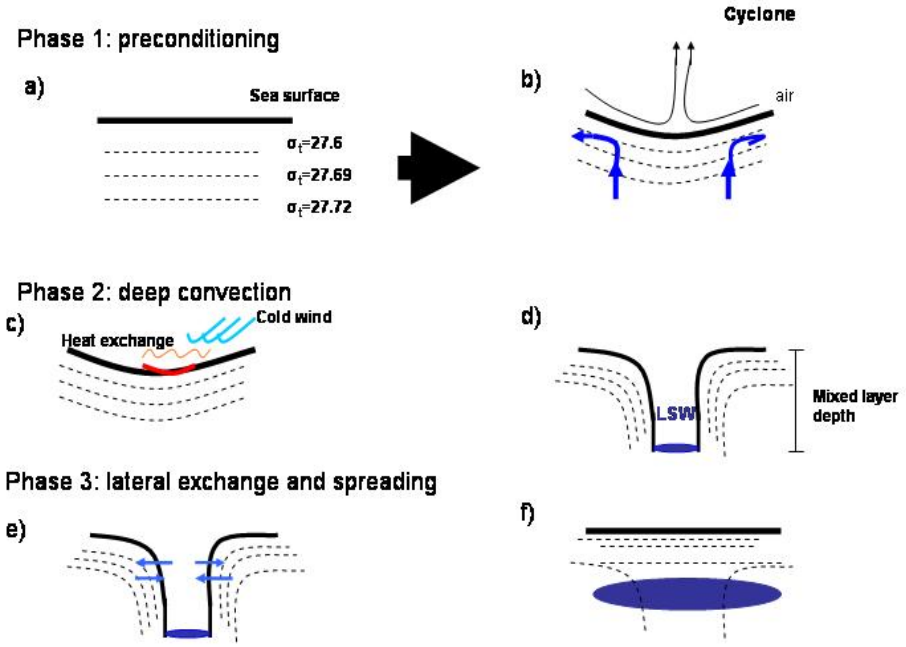

Figure 1.2. A simplified schematic diagram of the three phases of open ocean deep convection: (a) ocean cross section, (b) cyclonic condition , (c) atmospheric forcing (d) deep sinking (e) lateral exchange (f) spreading.

1.2(c)). Then a substantial part of the fluid column overturns in numerous plumes, less than 1 km scale. The height of this fluid column is the MLD (figure 1.2(d)). The dense surface water is redistributed in the vertical. The Labrador Sea Water (LSW) formed is dense water mass and sinks to the deeper ocean. The third phase is the lateral exchange and spreading of LSW (figure 1.2(e) and 1.2(f)). The upper ocean undergoes restratification and the water disperses under the influence of gravity and rotation, on a timescale of weeks to month. The second and third phrases do not necessarily happen sequentially but can occur simultaneously (Marshall and Schott 1999).

The cold wind from Canadian Arctic (atmospheric forcing), the cyclonic condition (Clarke and Gascard 1983) and the sea water properties (weakly stratified due to previous convection) of Labrador Sea make it especially favorable for deep convection.

Apart from the necessary conditions discussed in the previous sections, the North Atlantic Oscillation (NAO) index, strength of westerly winds, freshwater flux, heat flux, among other factors also determine the occurrence and intensity of the deep convection (Stramma *et al.* 2004).

1.4 Labrador Sea Water Formation and Dispersal

1.4.1 Mixed layer depths

The deep convection that occurred in the winters of 1990-1994 was potentially the strongest in this century (at least considering the available hydrographic data), which produced the MLD to approximately 2300 m. However from 1995-2001, deep convection was weak and the MLD produced are only just around 1000 m (Lazier *et al.* 2002). Lavender *et al.* (2002) found the deepest mixed layer depth exceeded 1300 m in 1997 but is less than 1000 m in 1998.

Hydrographic data (Clarke and Gascard 1983, LabSeaGroup 1998, Lavender *et al.* 2002) and modelling results (Mizoguchi *et al.* 2003) showed that the deepest mixed layer depths are found in the western Labrador Sea. But some studies also showed other regions of convection; such as Pickart and Torres (2001), who found deep convection on the western continental slope. Furthermore, with LSW formed directly entrained into the DWBC, during the winter of 1996-1997. Lavender *et al.* (2002) also observed that mixed layers located southwest of Cape Farewell and north of 60^oN.

1.4.2 Spreading of the LSW

Talley and McCartney (1982) first proposed three principle pathways of spreading of LSW: Spreading from Labrador Sea to the northeast into Irminger Sea; Spreading eastward or southeastward to earthen North Atlantic; Spreading with the DWBC, these have been widely adopted. The intensity of the deep convection and the amount of the LSW formed varies year to year and recently, there is evidence that deep convection sites may be changing (Curry *et al.* 2003).

Rhein *et al.* (2000) estimated CFC inventories to trace the LSW after the strong deep convection of 1994 winter. They found 31 % of the CFC inventory in the eastern Atlantic and only 28 % of that remained in interior Labrador Sea through 1997. This implied around one third of LSW spread from interior Labrodor Sea to eastern Atlantic within three years. By using an advective-diffusive model, Straneo *et al.* (2003) reported the two traditional spreading pathways which Clarke and Gascard (1983) defined (eastward and to DWBC) but also a new spreading pathway: spreading towards the West Greenland Coast from the interior by a strong recirculation. They also estimated that 80 % and only 20 % of LSW will spread into the DWBC and Irminger pathway (the eastward pathway), respectively, in approximately 4-5 years. There are also some evidences that deep convection might also occur in Irminger sea and the water mass formed there also contributes to the formation of the LSW (Pickart *et al.* 2003).

1.5 Measurement techniques and international program in physical oceanography

1.5.1 Basic principle

There are two principal approaches to observe ocean properties: Lagrangian and Eulerian. Suppose a trace particle is put into the ocean. Lagrangian observation gives the position of the particle at different times if the particle is allowed to flow freely in the ocean. Eulerian observation gives the water speed and direction at a particular location. The former one can provide the trajectories of the particle while the latter can provide instantaneous velocity vectors in a fixed location.

The Argo floats we used in this work are based on a Lagrangian approach.

1.5.2 ARGO

Argo is an acronym of Array for Real-time Geostrophic Oceanography and it is an international joint effort which maintains a network of floats throughout the world's ocean. Argo's history can be found from 1990-1997 World Ocean Circulation Experiment (WOCE) which was under the World Climate Research Programme (WCRP). In it, there were approximately 1000 Autonomous Lagrangian Circulation Explorer (ALACE) floats measuring the global deep circulation. ALACE with sensors to measure the temperature and salinity in the vertical is called Profiling-ALACE (PALACE) and different versions of this are being used by Argo. The working principle of the PALACE floats is that the floats start on the ocean surface and then sink downward to 2000 meters. Then they drift for ten days and thereafter, they rise to the surface. Temperature and salinity profiles are recorded while they are rising. The position of the floats combined with the profiles will be sent to a satellite and then to a data processing center in near real-time (Wilson 2000) . The buoyancy of the float is controlled by pumping oil into or out from an external bladder (Davis *et al.* 2001).

Under the Argo project, each member country maintains its own floats. Through September of 2004, the USA was operating 733 Argo floats, Japan has 225 floats and the European Union has 294. The total number of floats in the water was 1452, which is about 50 % of the target number of 3000 proposed for a sustainable float array to be in place by 2006.

For the Canadian Argo, currently there are 84 floats, which are managed by the Department of Fisheries and Oceans of Canada. The Canadian float is the APEX (Autonomous Profiling Explorer) float produced by Webb Research Corp. It basically work like the Sounding Oceanographic Lagrangian Observer (SOLO) floats which is an improved version of ALACE floats, with full depth control (Davis *et al.* 2001). Its lifetime is about 5 years and its weight is 26 kg. The float is cylindrical and has 16.5 cm diameter and 130 cm length and is equipped with a 70 cm antenna. It can collect 80-100 temperature and salinity profiles over its deployment lifetime. The accuracy is about 0.1^oC in temperature and 0.01 psu in salinity (Canadian Department of Fisheries and Oceans, available online at: www.dfo-mpo.gc.ca).

1.6 Introduction to oceanic general circulation model

The fundamental equations of the numerical ocean modelling are based on the Naiver-Stokes equations. These equations, as known as the primitive equations are solved principally to give values of the seven variables: ρ, u, v, w, T, S, p which are the sea water density, velocity in x direction, velocity in y direction, velocity in z di-

rection, temperature, salinity and pressure respectively in the Cartesian coordinate system.

u, v can be calculated from the horizontal momentum equations given by:

$$\partial_t u + \vec{v} \cdot \bigtriangledown u - fv - \bigtriangledown \cdot A \bigtriangledown u = -\frac{1}{\rho} \partial_x p \tag{1.1}$$

$$\partial_t v + \vec{v} \cdot \bigtriangledown v + fu - \bigtriangledown \cdot A \bigtriangledown v = -\frac{1}{\rho} \partial_y p \tag{1.2}$$

while the equation for computing w can be derived from the continuity equation,

$$\partial_z w = -\partial_x u - \partial_y v \tag{1.3}$$

where $\vec{v} = (u, v, w)$. On the left hand side of the first two equations, the first term is the local acceleration while the second term is the momentum advection. The third term is the Coriolis term where f is the Coriolis parameter, which is equal to $2\Omega \sin \phi$, Ω is the angular velocity of the earth and ϕ the latitude. The fourth term is the viscosity term, A is the matrix of horizontal and vertical turbulent coefficients.

The term on the right hand side of the above three equations is the pressure gradient.

The tracers, T and S can be computed from the advection diffusion equations given by:

$$\partial_t T + \vec{v} \cdot \bigtriangledown T = \bigtriangledown \cdot K \bigtriangledown T \tag{1.4}$$

and

$$\partial_t S + \vec{v} \cdot \bigtriangledown S = \bigtriangledown \cdot K \bigtriangledown S \tag{1.5}$$

where the second term of equation 1.4 and 1.5 is the advection term while the term on the right stands for the diffusion, t is time, K is the diffusion tensor.

and the p is computed with:

$$\partial_z p = -g\rho \tag{1.6}$$

and finally, ρ can be computed with the equation of state.

$$\rho = \rho(T, S, p) \tag{1.7}$$

To solve the above partial differential equations directly needs huge efforts and is nearly impossible. Therefore, approximations are used to simplify the equations such as the hydrostatic, Boussinesq and thin shell approximations (see Haidvogel and Beckmann (1999) and also the MOM manual available online: www.gfdl.noaa.gov/~smg/MOM/MOM_manual.html).

At present, the majority of the ocean models are based on finite differences. Finite difference models can be furthur classified into the geopotential (e.g. the Modular Ocean Model, MOM by the Geophysical Fluid Dynamics Laboratory, GFDL), the terrain-following (e.g. SCRUM, S-Coordinate Rutgers University Model by Rutgers U.) and isopycnic (e.g. MICOM, the Miami Isopycnic Coordinate Ocean Model, by the University of Miami) (Haidvogel and Beckmann 1999).

The model we used in this work is the sub-polar ocean model (SPOM) which was developed by Myers (2002*b*). SPOM is a regional region configuration of MOMA. The detail and the configuration of SPOM is discussed in Chapter 3.

1.7 The aims and the organization of the paper

Some studies suggest that anthropogenic global warming may cause climate change by weakening the North Atlantic and global meridional overturning (thermohaline) circulation and also by intensifying the global water cycle (e.g. Hakkinen and Rhines 2004). Some other studies, such as Dickson *et al.* (2003), pointed out that there is a freshening trend in the North Atlantic, not that the thermohaline circulation is being weakened. The real situation remains uncertain due to the high variability of deep convection and LSW in the Labrador Sea. Meanwhile, the Argo project provide us with high spatial data coverage with near real-time hydrographic data which help us to study such variability.

In this paper, we investigate deep convection and its product, LSW, as well as the circulation through the Labrador Sea during the winters of 2002 to 2004. This is carried out based on the observational data from Argo followed by modelling effort. In Chapter 2 of this paper, observational data based on Agro is discussed. We explore the inter-annual variability of the Labardor Sea based on a number of different fields. Important oceanic quantities such as the mixed layer depth, heat content and float trajectories are studied. In Chapter 3, a well developed finite difference

ocean model is introduced, then the model is used to simulate the behavior in the Labrador Sea during the same three winters of 2002 - 2004. Comparison with the observations are made to reveal the limitation of the modelling study. Then, we discuss the model results. Finally, Chapter 4 is an overall summary and discussion.

2 Interannual study of the Labrador Sea

2.1 Data Set

The Argo float data servers are in the USA and in France, the two of them carrying identical versions of the Argo data sets. Our float data are obtained from the US Server and the data are in netCDF format.

In this paper, we focus on the region bounded by 45^oN to 65^oN and 40^oW to 70^oW. This domain allows us to focus on the entire Labrador Sea. We have two definitions for winters: a 'short' winter is defined to be from January to March; a 'long' winter is defined to be from the previous year's November to the existing year's May. The long winter definition has been added to give us a longer study period with more floats reporting.

Quality control is made for all profiles by visual inspection. Some of the floats falling in our interested region did not record proper temperature or salinity profiles and therefore were discarded (this might be caused by sensor failure, signal transmitting failure or recording failure, etc.). Linear interpolation is used on some of the profiles.

2.2 Potential temperature, salinity and potential density

The potential temperature, salinity and potential density are examined at 1000 m, 1500 m and 2000 m as LSW is generally present at these depths.

2.2.1 Potential temperature distribution at 1000 m, 1500 m, 2000 m

Figure 2.1, figure 2.2 and figure 2.3 show the potential temperature at 1000 m, 1500 m and 2000 m, respectively. The highest temperatures occur around 40^oN - 48^oN, 40^oW - 45^oW (the northwest corner region associated with the North Atlantic Current) in all the winters of the three successive years at all three different depths. These warmest waters may associate with the deep flows of the North Atlantic Current. Perez-Brunius *et al.* (2004) suggested that the cross-frontal mixing between

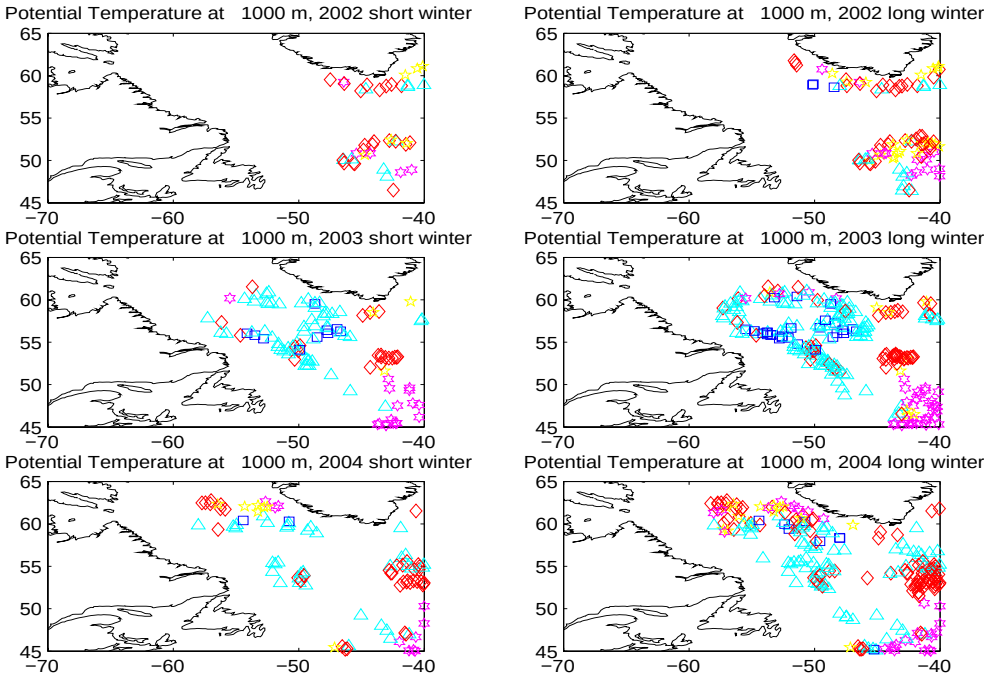

Figure 2.1. The potential temperature, θ at 1000 m in Labrador Sea. $\theta \leq 3^o$ C is marked green circles, $3 < \theta \leq 3.2^o$ C with blue squares, $3.2 < \theta \leq 3.4^o$ C with light blue triangles, $3.4 < \theta \leq 3.6^o$ C with red diamonds, $3.6 < \theta \leq 3.8^o$ C with yellow pentagons, and $\theta > 3.8^o$ C with purple hexagons

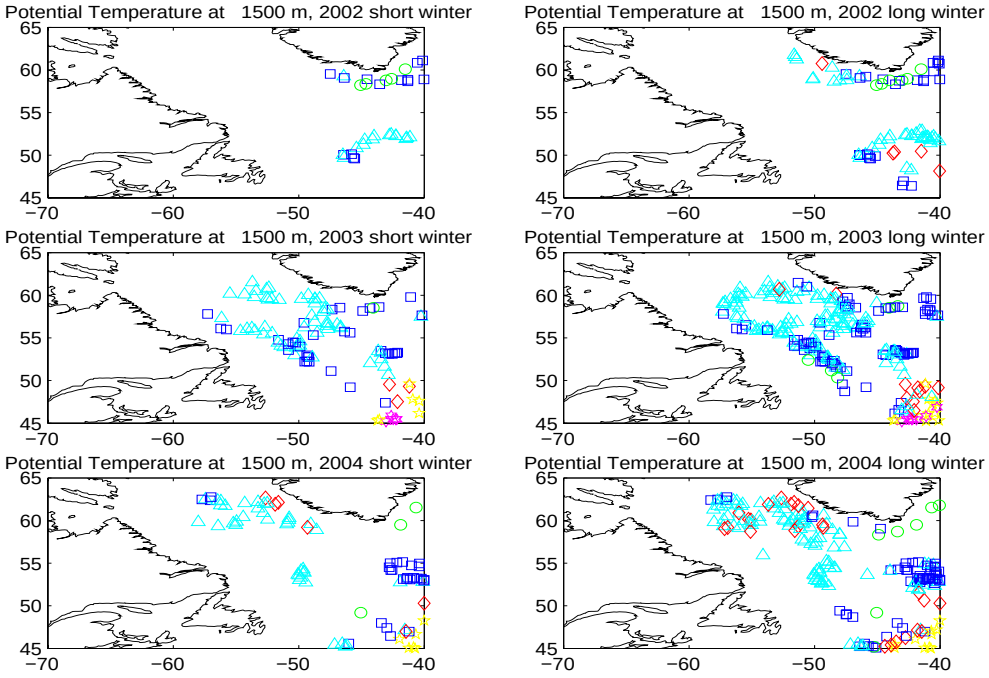

Figure 2.2. The potential temperature, θ at 1500 m in Labrador Sea. $\theta \leq 3^o$ C is marked green circles, $3 < \theta \leq 3.2^o$ C with blue squares, $3.2 < \theta \leq 3.4^o$ C with light blue triangles, $3.4 < \theta \leq 3.6^o$ C with red diamonds, $3.6 < \theta \leq 3.8^o$ C with yellow pentagons, and $\theta > 3.8^o$ C with purple hexagons

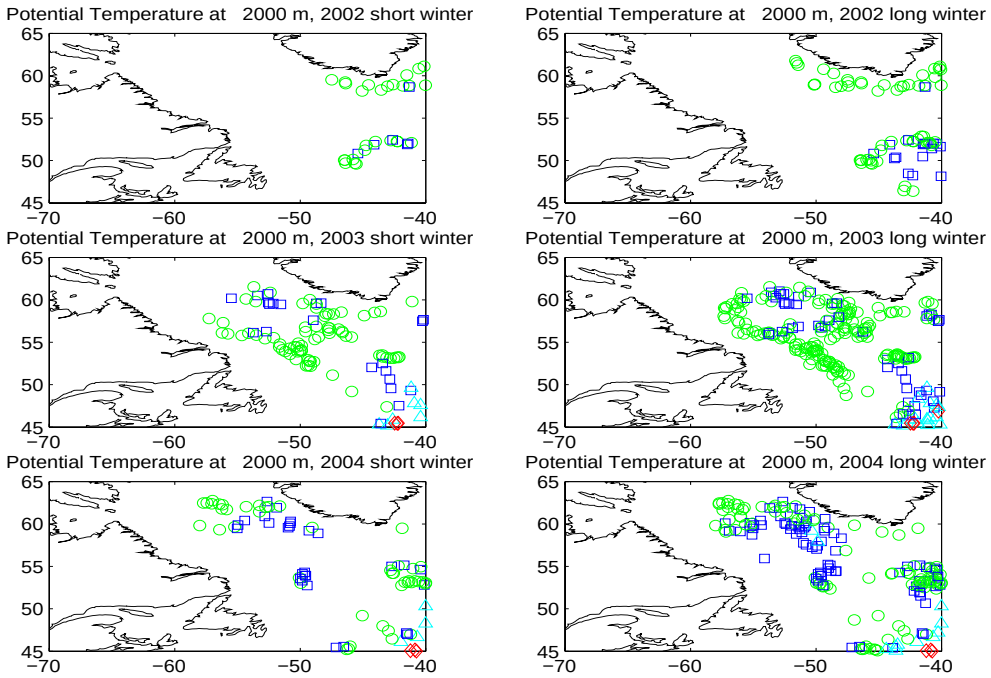

Figure 2.3. The potential temperature, θ at 2000 m in Labrador Sea. $\theta \leq 3^o$ C is marked with green circles, $3 < \theta \leq 3.2^o$ C with blue squares, $3.2 < \theta \leq 3.4^o$ C with light blue triangles, $3.4 < \theta \leq 3.6^o$ C with red diamonds, $3.6 < \theta \leq 3.8^o$ C with yellow pentagons, and $\theta > 3.8^o$ C with purple hexagons

the cold and fresh subpolar waters and the salty and warm salty NAC waters is the main mechanism for the light to dense water transformation process when NAC enter the western subpolar region. This mixing process may also be a reason for those warmest temperatures to present.

At 1500 m and 2000 m, in the three successive winters, there are relatively lower temperatures occurring along the east coast and tip but relatively higher temperature occurring along the west coast of Greenland. The east coast low temperatures reveal the water from the Arctic, while the west coast high temperatures show a mixture of water from the Arctic and the Irminger Sea Water (ISW) brought by the Irminger Current offshore of the WGC. Furthermore, one might notice that there is a small group of relatively low temperatures at around 63^oN at 2004 winters, only at 1500m and 2000m. This suggests that there may be some colder water masses coming out from Davis Strait. These low temperatures do not associate with low salinities (figure 2.5 and 2.6).

Generally, the majority of the profiles has temperatures in the range $3.2 - 3.4^o$C range in all years at 1000 m and 1500 m. From figure 2.1, in the central Labrador Sea region (around 55^oN - 57^oN, 53^oW - 50^oW), there is a group of temperatures with $3 - 3.2^o$C (blue squares) in the winters of 2003. This may due to recirculation

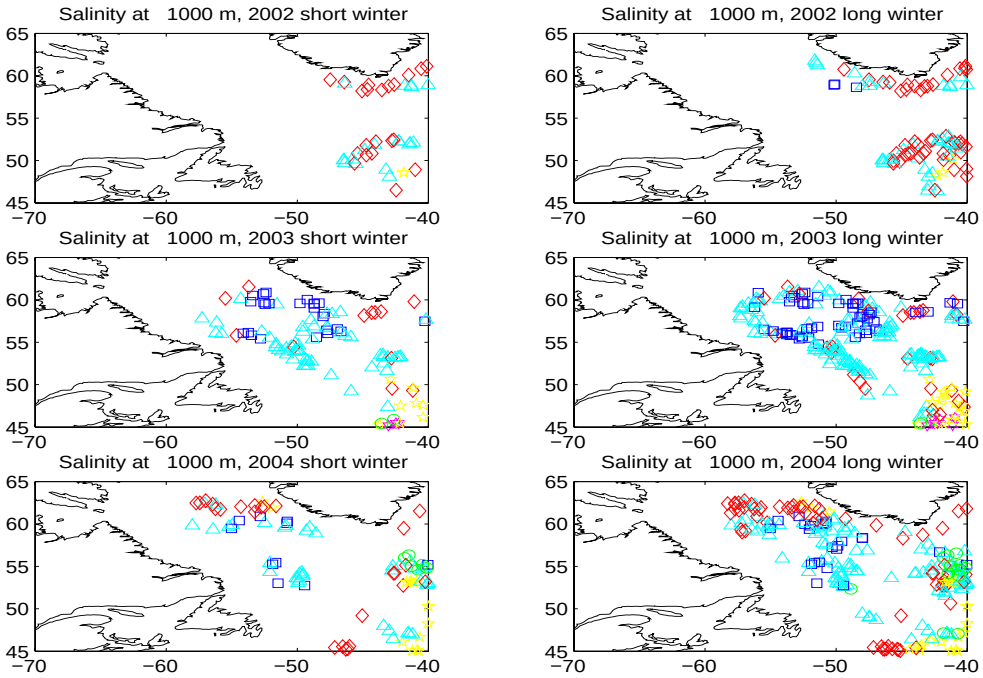

Figure 2.4. The salinity, s at 1000 m in Labrador Sea. $s \leq 34.8$ psu is marked with green circles, $34.8 < s \leq 34.84$ psu with blue squares, $3.84 < s \leq 34.88$ psu with light blue triangles, $34.88 < s \leq 34.92$ psu with red diamonds, $34.92 < s \leq 35$ psu with yellow pentagons, and $s > 35$ psu with purple hexagons

which brings warmer water to the interior. Although in the same region, there is some of the deepest convection (figure 2.15). Therefore, these temperatures might also relate to the deepest convection. There are no data in the 2002 winter in that region. For 2004, the $3 - 3.2^{o}$C temperature profiles are occurring relative more northerly.

2.2.2 Salinity distribution at 1000 m, 1500 m, 2000 m

Like the potential temperature, the salinity is relatively higher in the southeast region than in the rest of the area. This occurs only at 1000 m and 2000 m. Another high salinity region is the west coast of Greenland. Again it is due to the inflowing of the ISW brought by the Irminger current. There is more warm ISW inflow present in 2004 than in 2003.

The high salinity around 43^{o}N agrees with Stramma *et al.* (2004) who suggest there is a mixing process going on in the southern subpolar region. From 56^{o}N down to 48^{o}N, the sea water is generally fresher due to convectively formed water, especially in 2003.

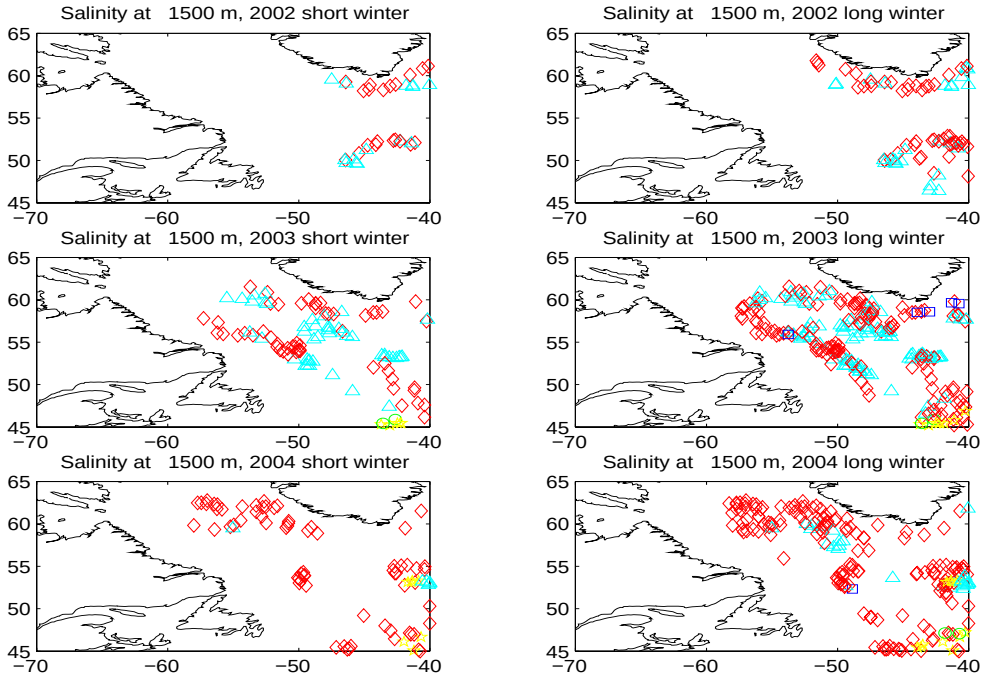

Figure 2.5. The salinity, s at 1500 m in Labrador Sea. $s \leq 34.8$ psu is marked with green circles, $34.8 < s \leq 34.84$ psu with blue squares, $3.84 < s \leq 34.88$ psu with light blue triangles, $34.88 < s \leq 34.92$ psu with red diamonds, $34.92 < s \leq 35$ psu with yellow pentagons, and $s > 35$ psu with purple hexagons

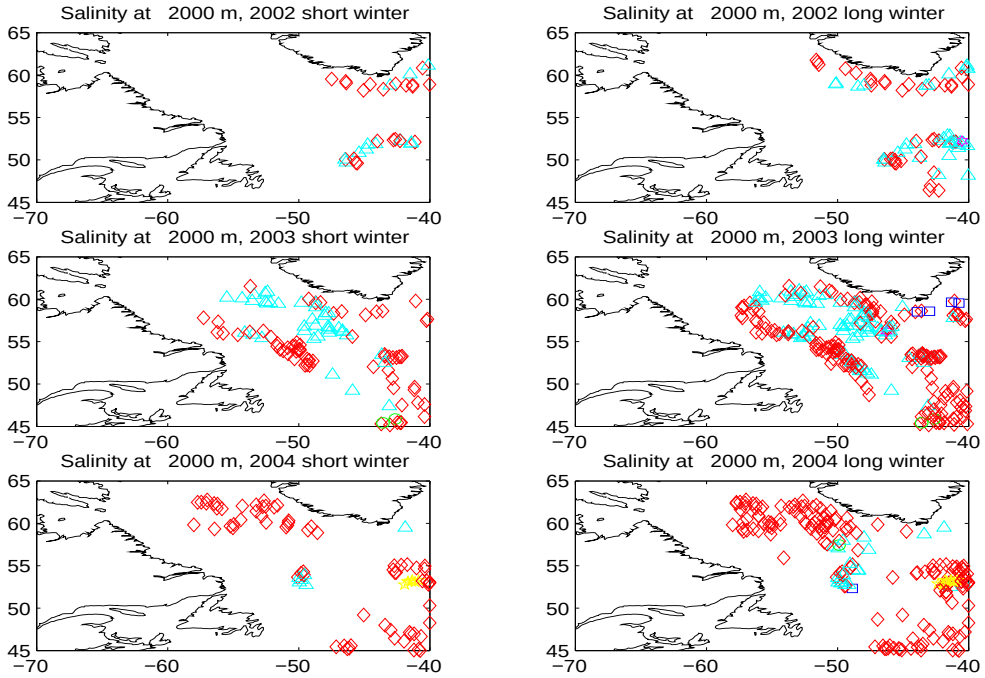

Figure 2.6. The salinity, s at 2000 m in Labrador Sea. $s \leq 34.8$ psu is marked with green circles, $34.8 < s \leq 34.84$ psu with blue squares, $3.84 < s \leq 34.88$ psu with light blue triangles, $34.88 < s \leq 34.92$ psu with red diamonds, $34.92 < s \leq 35$ psu with yellow pentagons, and $s > 35$ psu with purple hexagons

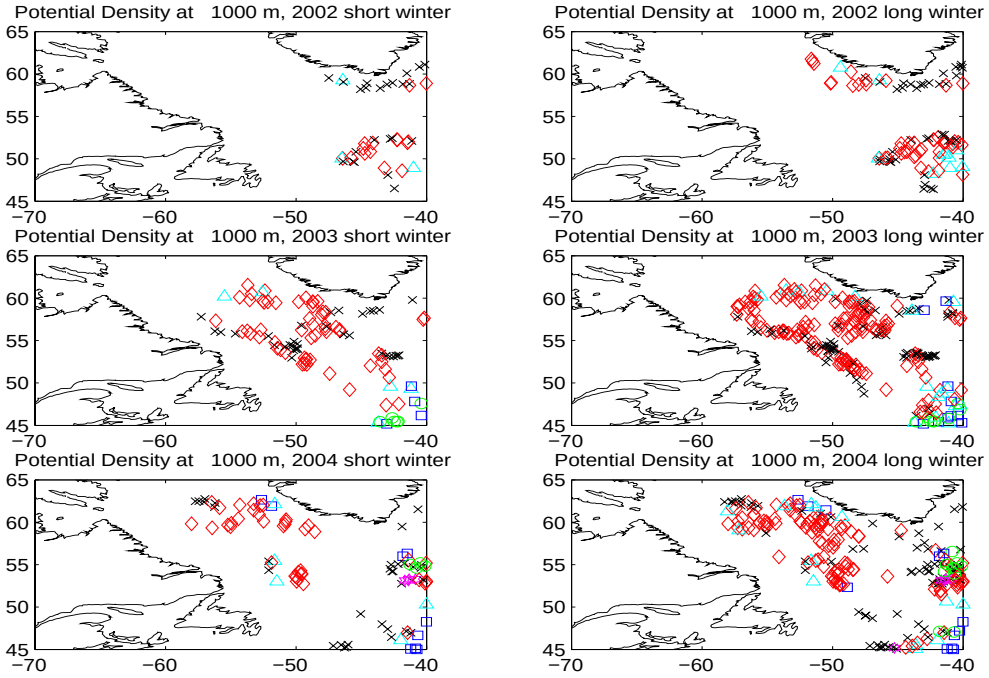

Figure 2.7. The potential density, σ_θ at 1000 m in Labrador Sea. $\sigma_\theta \leq 27.65$ kgm^{-3} is marked with green circles, $27.65 < \sigma_\theta \leq 27.7$ kgm^{-3} with blue squares, $27.7 < \sigma_\theta \leq 27.74$ kgm^{-3}with light blue triangles, $27.74 < \sigma_\theta \leq 27.76$ kgm^{-3} with red diamonds, $27.76 < \sigma_\theta \leq 27.78$ kgm^{-3} with yellow pentagons, $27.78 < \sigma_\theta \leq 27.8$ kgm^{-3} with black cross, and $\sigma_\theta > 27.8$ kgm^{-3} with purple hexagons

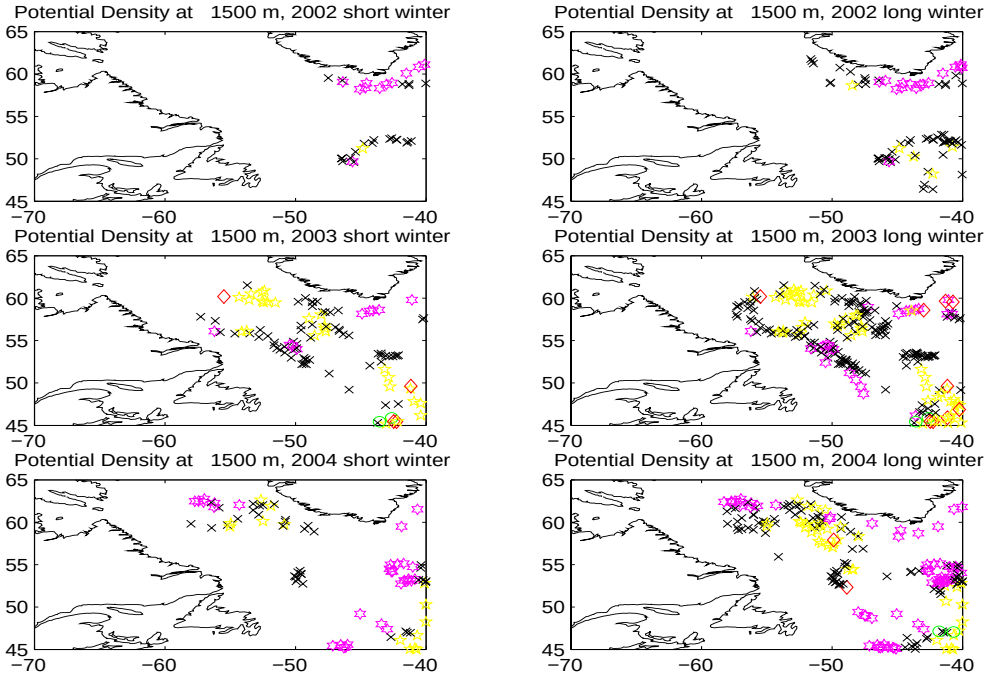

Figure 2.8. The potential density, σ_θ at 1500 m in Labrador Sea. $\sigma_\theta \leq 27.7$ kgm^{-3} is marked with green circles, $27.7 < \sigma_\theta \leq 27.72$ kgm^{-3} with blue squares, $27.72 < \sigma_\theta \leq 27.74$ kgm^{-3}with light blue triangles, $27.74 < \sigma_\theta \leq 27.76$ kgm^{-3} with red diamonds, $27.76 < \sigma_\theta \leq 27.78$ kgm^{-3} with yellow pentagons, $27.78 < \sigma_\theta \leq 27.8$ kgm^{-3} with black cross, and $\sigma_\theta > 27.8$ kgm^{-3} with purple hexagons

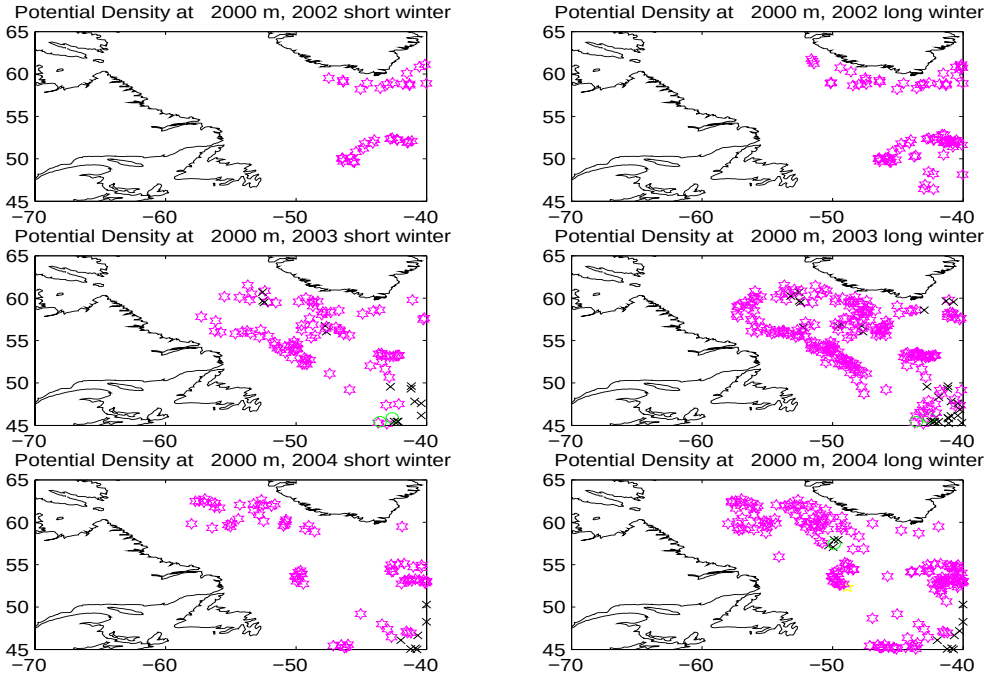

Figure 2.9. The potential density, σ_θ at 2000 m in Labrador Sea. $\sigma_\theta \leq 27.7$ kgm^{-3} is marked with green circles, $27.7 < \sigma_\theta \leq 27.72$ kgm^{-3} with blue squares, $27.72 < \sigma_\theta \leq 27.74$ kgm^{-3}with light blue triangles, $27.74 < \sigma_\theta \leq 27.76$ kgm^{-3} with red diamonds, $27.76 < \sigma_\theta \leq 27.78$ kgm^{-3} with yellow pentagons, $27.78 < \sigma_\theta \leq 27.8$ kgm^{-3} with black cross, and $\sigma_\theta > 27.8$ kgm^{-3} with purple hexagons

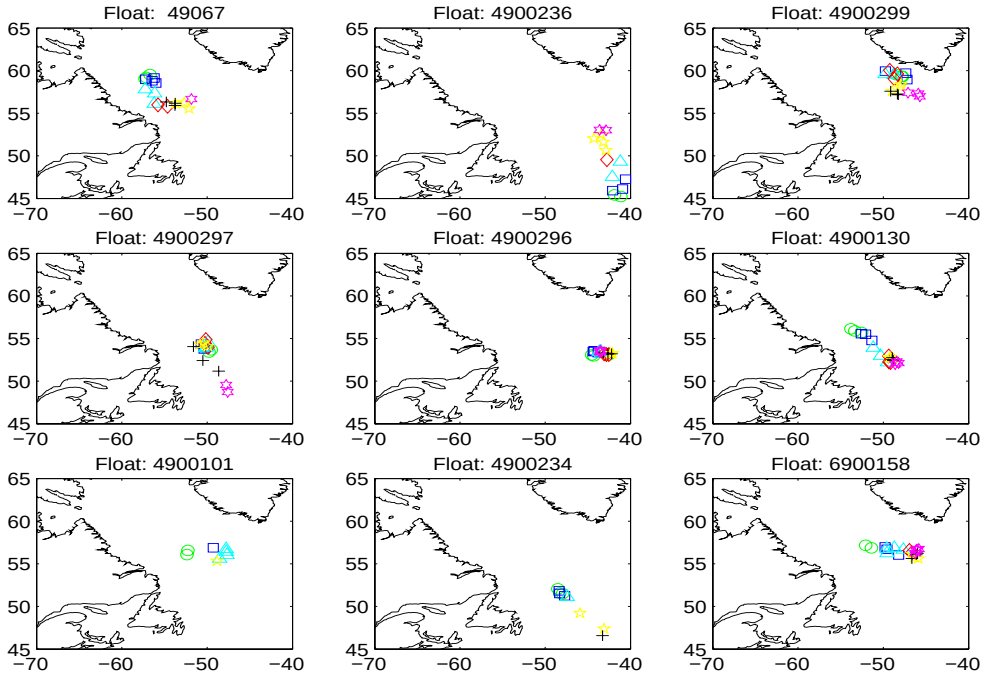

Figure 2.10. Spreading paths of LSW (σ_θ between 27.74 and 27.8) at 1500m in 2003 long winter: green circles denote profiles in November, light blue triangles denote profiles in December, blue squares denote profiles in January, red diamonds denote profiles in February, yellow pentagons denotes profiles in March, black crosses denotes profiles in April and purple hexagons denote profiles in May

2.2.3 Potential density distribution at 1000 m, 1500 m, 2000 m

We define LSW as the water between isopycnals of 27.74 and 27.8 kgm^{-3}. In all the density plots (figure 2.7, 2.8 and 2.9), the red diamonds, yellow pentagons and the black crosses all represent LSW. When moving down from 1000 m to 1500 m (from figure 2.7 to figure 2.8), the LSW along the southeast coast of Greenland disappear while there are more LSW found in the NAC region. We can find almost no LSW at 2000 m (figure 2.9).

At 1000 m, there are mainly two dictinct water masses: 27.74 - 27.76 kgm^{-3} (red diamond) and 27.78 - 27.8 kgm^{-3} (black cross).

Spreading of LSW

We roughly trace the LSW by plotting the time series of the location of potential density ranging from 27.74-27.8 at 1500 m. To do this we assume the water flow

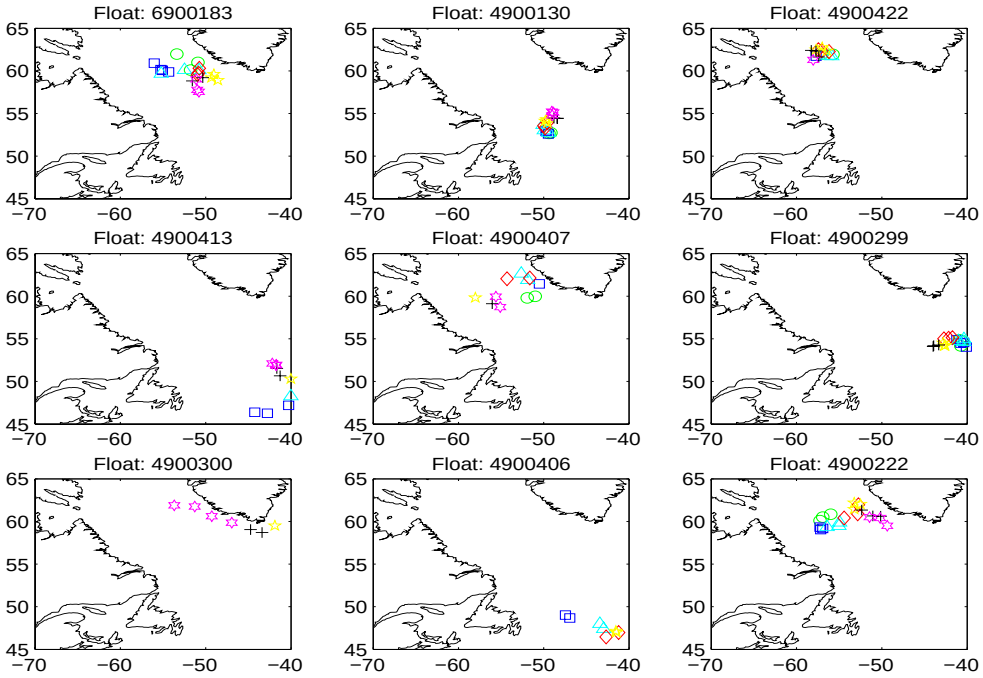

Figure 2.11. Spreading paths of LSW (σ_θ between 27.74 and 27.8) at 1500m in 2004 long winter: green circles denote profiles in November, light blue triangles denote profiles in December, blue squares denote profiles in January, red diamonds denote profiles in February, yellow pentagons denotes profiles in March, black crosses denotes profiles in April and purple hexagons denote profiles in May

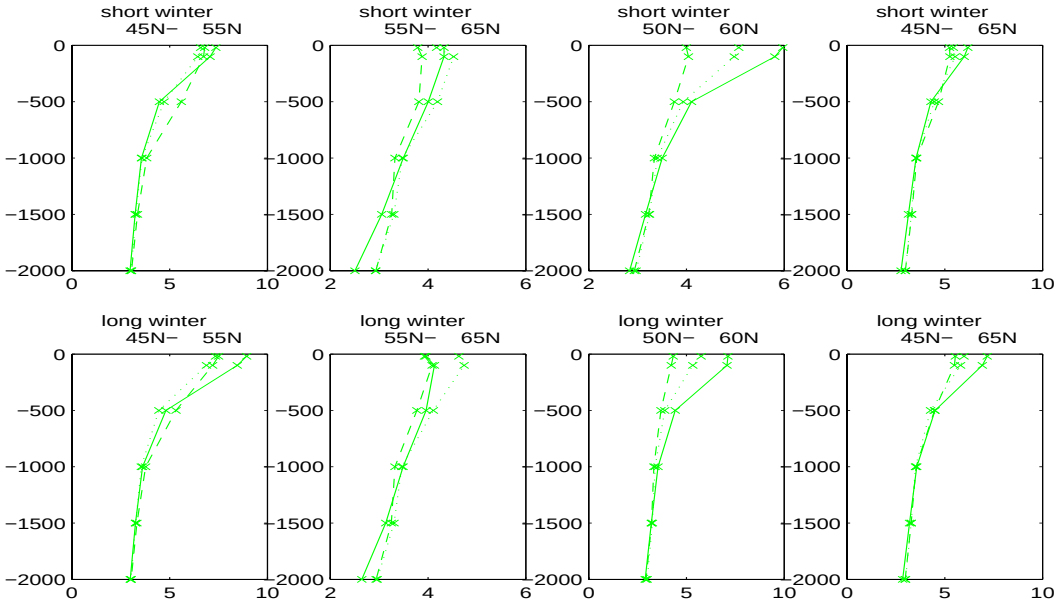

Figure 2.12. The average θ vs depth in different regions of Labrador Sea (Latitude range), unit: ^{o}C, a filled line denotes 2002, a dash line denotes 2003, a dotted line denotes 2004.

is barotropic between 1500 m and 2000 m since the floats drift at 2000 m. The paths of spreading of LSW in 2003 and 2004 are shown in figure 2.10 and figure 2.11 respectively. In 2003, Float 49067, 4900297, 4900130 and 4900234 generally follow the classical DWBC spreading pathway, while Float 6900158 and Float 4900101 show another classical spreading pathway, i.e. spreading eastward. In 2004, Float 4900222 shows LSW spreading from the Labrador shelf to the west Greenland shelf. This might be achieved by a counter current. This is similar to the simulation result of Straneo *et al.* (2003). At the same time, Float 4900300 shows LSW spreading along the Greenland coast from the Irminger Sea.

2.2.4 Average values in 55N - 65N, 55N - 65N, 50N - 60N and 45N - 65N

The average values of potential temperature, salinity and potential density based on all profiles in each winter are computed at 20 m, 100 m, 500 m, 1000 m, 1500 m and 2000 m on four different sub-regions of Labrador Sea, which is determined with latitude ranges: 45^{o}N - 55^{o}N (the southern Labrador Sea); 55^{o}N - 66^{o}N (the northern Labrador Sea); 50^{o}N - 60^{o}N (the central Labrador Sea); 45^{o}N - 65^{o}N (the whole region).

In figure 2.12, among the four regional bands, 50^{o}N - 60^{o}N(the central Labrador

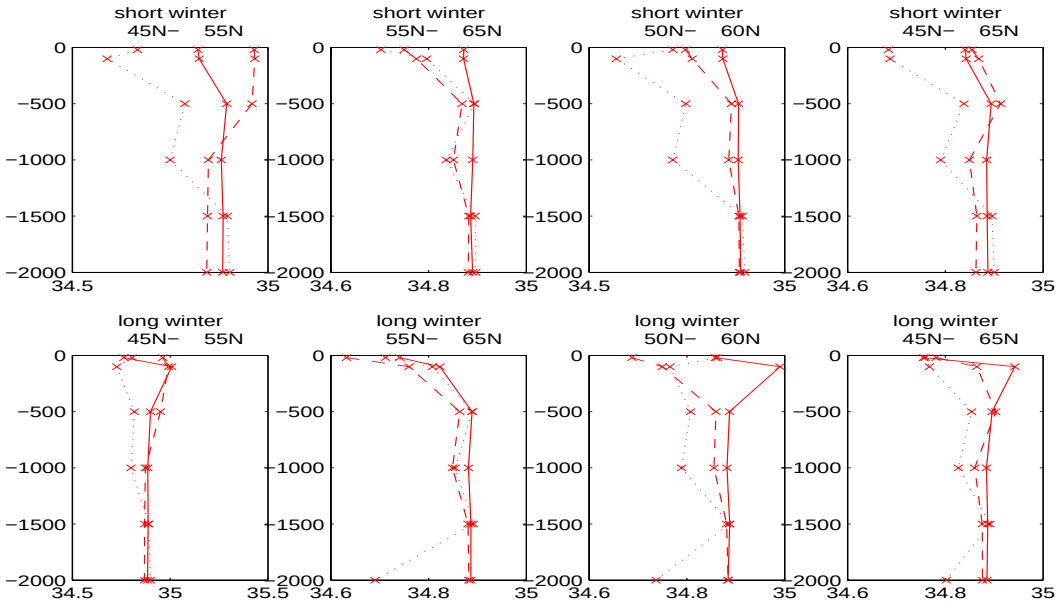

Figure 2.13. The average salinity vs depth in different regions of Labrador Sea (Latitude range), unit: psu, a filled line denotes 2002, a dash line denotes 2003, a dotted line denotes 2004.

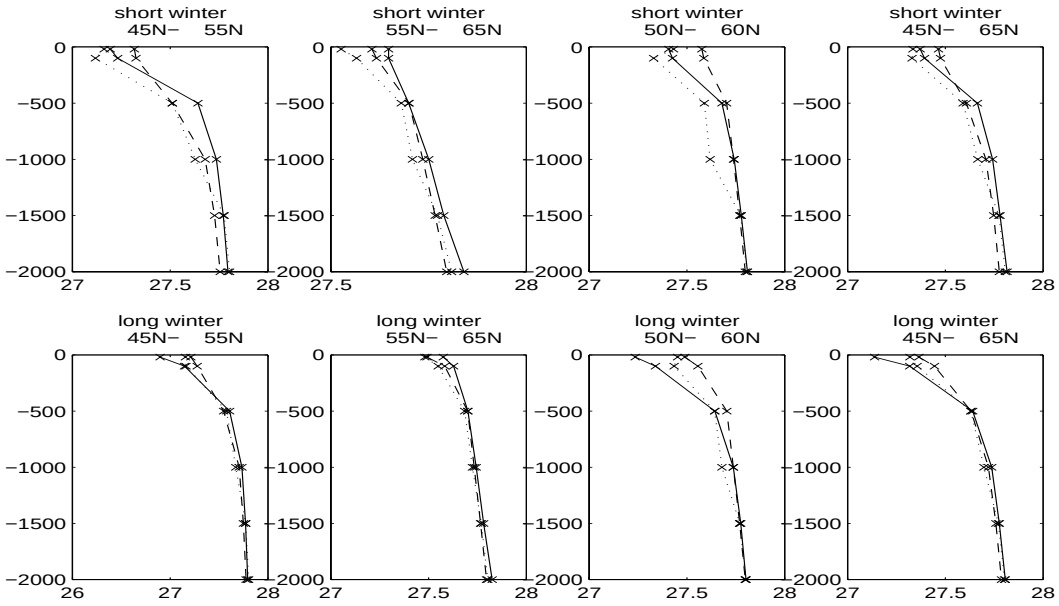

Figure 2.14. The average σ_θ vs depth in different regions of Labrador Sea (Latitude range, unit: kgm^{-3}, a filled line denotes 2002, a dash line denotes 2003, dotted line denotes 2004.

Sea) is the only region which shows $\theta_{2003} < \theta_{2002}$ and θ_{2004} distinctly at the upper 1000 m region. This is due to 2003 having the strongest deep convection (refer to next section) in that band. The lowest average temperature in 2003 is due to the low temperature of the convectively formed water.

Referring to figure 2.13, the average salinity of the southern Labrador Sea (45^oN - 55^oN) is relatively higher than other regions and this agrees with Stramma *et al.* (2004). However, the lowest salinity in 50^oN - 60^oN of 2004 is unexpected since the lowest salinity should arise in 2003 (the strongest convection year). Moreover, the average salinity may indicate a freshening trend of the upper ocean in these three years, especially on 50^oN - 60^oN band. The upper oceans of 2004 short winter on 45^oN - 55^oN and 50^oN - 60^oN are particular fresh compared to other years and other regions, this suggests there would be some freshening sources, such as precipitation. Though it is surprising that the 55^oN - 65^oN band have not been freshened in 2004.

Figure 2.14 shows that the difference of average σ_θ between each year in different bands is small almost at all depths. The largest difference could be seen on 50^oN - 60^oN, 2004, which shows the least dense water at the upper ocean and this is related to the particularly low salinity at this band.

In 2003, the stratification is weak in all regions. This suggests that there are more convection (refer to the next section). The greater upper layer density mainly is linked to colder temperatures, and higher salinities in this year.

2.3 Mixed layer depth

The mixed layer depth (MLD) can be estimated in various ways. We estimate the MLD using a simple density-criterion: the depth where the potential density is higher than that of the surface by a criterion density difference is defined as MLD.

We first use 0.03 kgm^{-3} as the criterion and then 0.02 kgm^{-3} to get two sets of MLD. We do this because we want to estimate the sensitivity of the results to the criterion choice. Both criteria basically give about the same results and plots. Figure 2.15 shows the distributions and the levels of MLD using 0.03 kgm^{-3} criterion and table 2.1 shows the statistic of estimated MLD. According to this, 2003 has the strongest deep convection as it has the higher proportion of deep MLD in the western Labrador Sea, offshore the boundary current where it is a traditional site for convection. Lavender *et al.* (2002) showed that the deepest MLDs in 1997 are found in about the same location, but with maximum value of 800 m. Nonetheless, there are some unexpected deep MLDs around 47kgm^{-3}N, 42kgm^{-3}W, where is also

Table 2.1. Mixed layer depth statistic

criterion	-	$0.03 kgm^{-3}$	$0.03 kgm^{-3}$	$0.02 kgm^{-3}$	$0.02 kgm^{-3}$
winter	profile	MLD > 600 m	MLD > 800 m	MLD > 600 m	MLD > 800 m
short winter 2002	42	3	1	2	1
long winter 2002	94	5	2	3	2
short winter 2003	108	11	3	7	2
long winter 2003	251	19	9	12	6
short winter 2004	96	2	1	1	1
long winter 2004	235	2	1	1	1

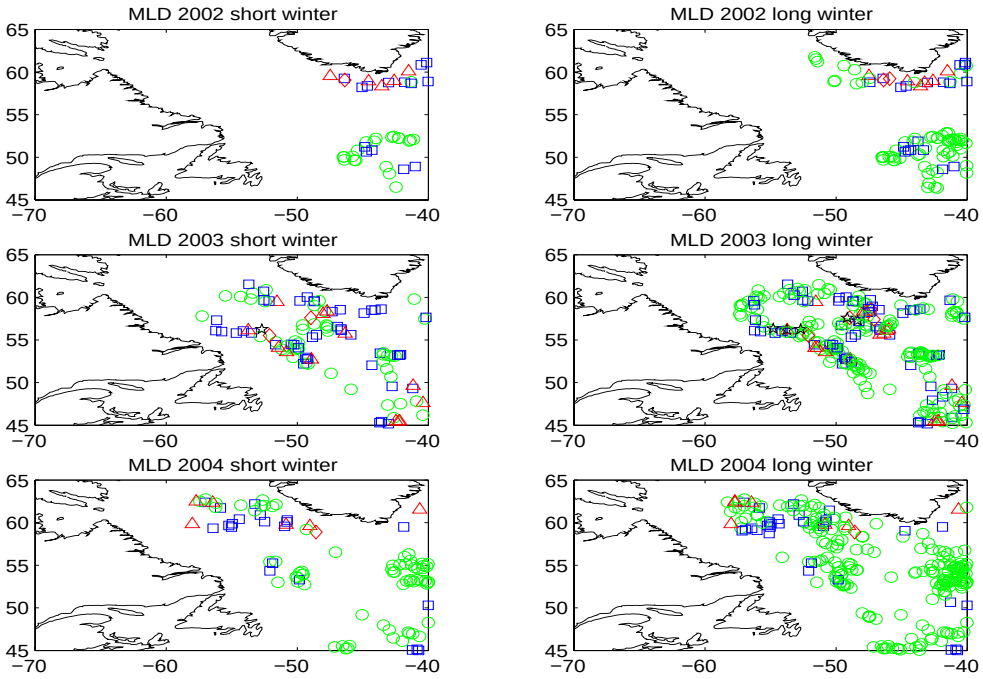

Figure 2.15. The mixed layer depth, MLD in Labrador Sea. MLD $\leq$ 200 m is marked with green circles, 200 $<$ MLD $\leq$ 500 m with blue squares, 500 $<$ MLD $\leq$ 800 m with light purple triangles, 800 m $<$ MLD $\leq$ 1100 m with red diamonds, 1100 m $<$ MLD $\leq$ 1600 m with black pentagons, and MLD $>$ 1600 m with purple hexagons

a high temperature region.

2002 might have a chance to have had stronger deep convection than 2003 but we do not have data on the central and the western Labrador Sea for 2002, which are extremely important for deep convection. However, from all the profiles we have, 2003 have the highest proportion of high MLDs which exceed 800 m (see table 2.1). Furthermore, the average MLD value in the whole region is the highest in 2003 (see table 2.2) and therefore we suggest that 2003 has the strongest deep convection among these three years. The year 2002 has stronger deep convection than 2004

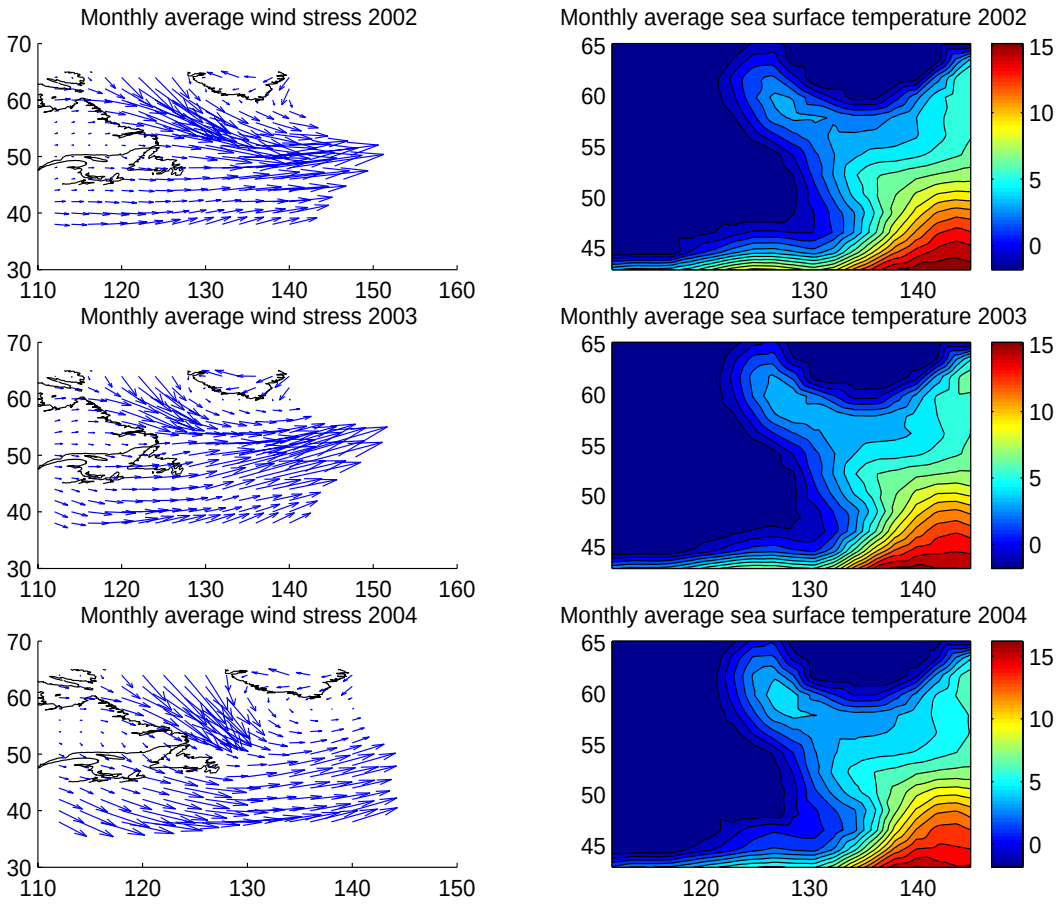

Figure 2.16. The monthly average (January to March) of wind stress and sea surface temperature.

as its proportion of deep MLD and average value in 50^oN-60^oN (see table 2.2) are higher.
The deep MLDs of 2002 are found off the southern tip of Greenland and they were mainly occurring in the short (Jan-Mar) winter, though we do not have data on either the western or the central Labrador Sea. Those deep MLDs in 2002 is not surprising as Lavender *et al.* (2002) have observed deepest MLDs located southwest of Cape Farewell.

In 2004, the location of deep MLDs shift northwestward relative to that of 2003. There were a few deep MLDs around 63^oN, we did not expect this as the cold and fresh water coming out from Davis Strait will hinder deep convection.

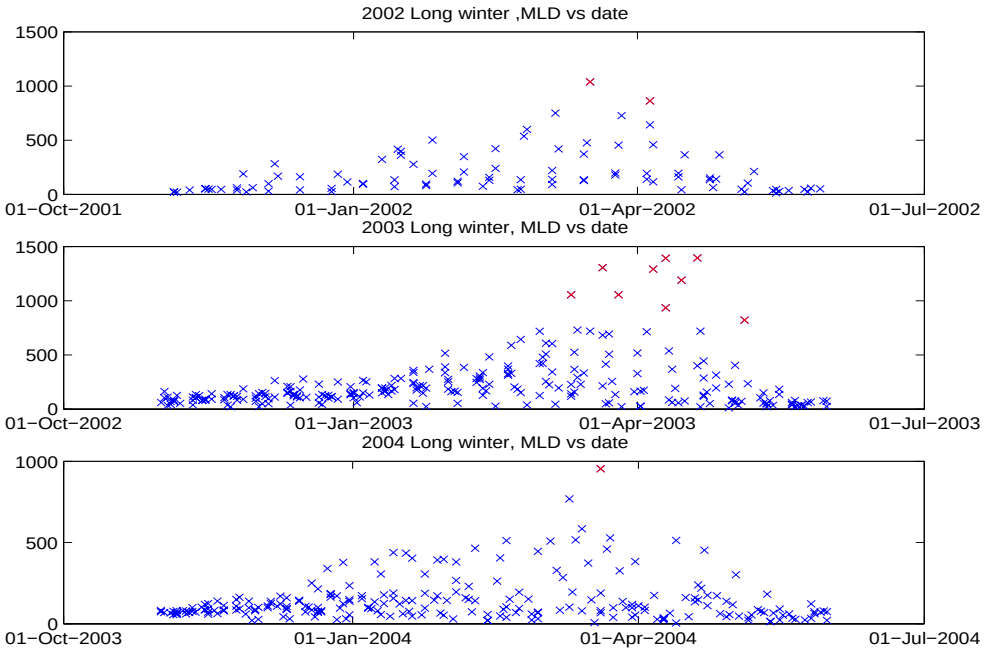

Figure 2.17. Time Series of MLDs from 2002-2004 with 0.03 kgm^{-3} density criterion, red crosses emphasise MLD $>$ 800 m

Was the convection in 2002 stronger than that in 2003 ?

The distribution of the monthly average (January to March) wind stress and sea surface temperature is shown in figure 2.16. The data are obtained from NCEP. 2003 has larger area of high sea surface temperature in the Labrador Sea than 2002 does. The winds mainly chill and hit the central Labrador Sea in 2003 rather than 2002 and 2004. The larger area of warm sea surface and more focusing wind chill in the central Labrador Sea in 2003 enhance more heat exchange between the atmosphere and the ocean, therefore this further suggests that there is stronger deep convection in 2003 than in 2002. In 2004, the location having higher sea surface temperature at around 60 ^{o}N is consistent with the location of the high MLD distribution there.

The time series of the MLD generally agree with the one found by Lavender *et al.* (2002); (their Fig 9) for 1996 - 1997 winter. From our result, the deep MLDs occur from the mid-February to the beginning of May, while the deep MLD vanished in 96 - 97 winter on the mid-April. This period also suggests that the deepest MLDs are found in late winter (mid to late April), with weak stratification post convection and restratification not finished

Table 2.2. Average MLD in different regions, unit (m)

Winter	45N-55N	55N-65N	50N-60N	45N-65N(whole region)
0.03 kgm^{-3} criterion				
2002 short winter	155	311	232	230
2002 long winter	122	221	178	164
2003 short winter	258	261	261	259
2003 long winter	180	195	196	188
2004 short winter	127	277	211	201
2004 long winter	99	184	150	144
0.02 kgm^{-3} criterion				
2002 short winter	146	280	209	210
2002 long winter	113	193	157	147
2003 short winter	236	218	220	227
2003 long winter	161	159	161	160
2004 short winter	116	229	183	172
2004 long winter	90	154	130	124

2.4 Heat content

The heat content of the heat energy the ocean possesses is crucial to the interaction with the climate system, the water mass formation process, heat transport of the ocean and heat flux. It can be used to constrain various ocean models.

The heat content (HC) above 1000 m, 1300 m and 1600 m is computed by the following equation:

$$HC = \rho_\circ C_p \int_{z_\circ}^{0} \theta(z) dz \tag{2.1}$$

For discrete data, the above equation is transformed to the following equation based on finite differences.

$$HC = \rho_\circ C_p \sum_{z_\circ}^{0} \frac{\theta_{n+1} + \theta_n}{2} (z_{n+1} - z_n) \tag{2.2}$$

where $\rho_\circ$ denotes the reference sea water density which is 1027.1 kgm^{-3} and C_p denotes the specific heat of water which is equal to 4000 (J kg^{-1} K^{-1}). z is the depth

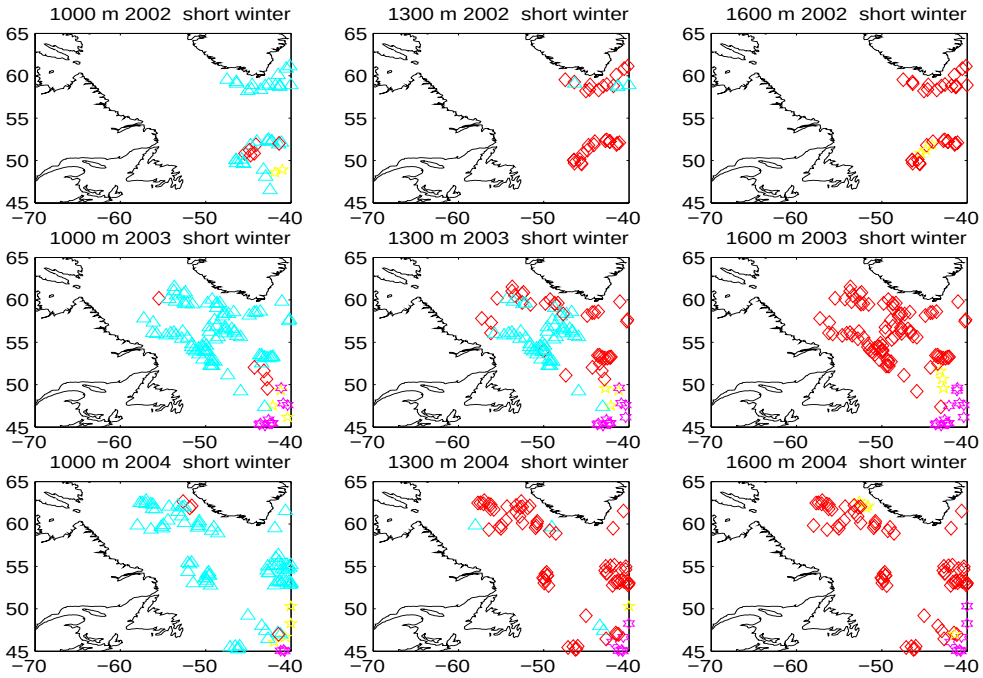

Figure 2.18. The heat content, HC above 1000 m, 1300 m, and 1600 m in the short winter (Jan - March winter). $0 < HC \leq 1 \times 10^{10}$ Jm^{-2} is marked with blue squares, $1 \times 10^{10} < HC \leq 2 \times 10^{10}$ Jm^{-2} with light blue triangles, $2 \times 10^{10} < HC \leq 3 \times 10^{10}$ Jm^{-2} with red diamonds, $3 \times 10^{10} < HC \leq 4 \times 10^{10}$ Jm^{-2} with yellow pentagons, and $HC > 4 \times 10^{10}$ Jm^{-2} with purple hexagons

while θ is temperature. $z_\circ$ is the desired depths: 1000 m, 1300 m or 1600 m.

Figure 2.18 and 2.19 show the heat contents of short (January-March) and long (November-May) winters respectively for the three successive years. For all the winters, the heat content mainly ranges from 1×10^{10} to 2×10^{10} Jm^{-2} (light blue triangles) at 1000 m, and range from 1×10^{10} to 2×10^{10} Jm^{-2} (red diamonds) at 1300 m and 1600 m. But at 1000 m in 2003 winters, there are a number of low heat content data in the southeast Labrador Sea. This suggests that the water masses between 1000 m to 1300 m in that region in year 2003 contain less heat compared to that in 2004. Furthermore, it is consistent with the strong convection occurring in 2003 respective to these three years since the newly convectively formed water is relatively colder and possesses less heat. While comparing the heat content of short winters to long winters, at 1300 m in 2004, there is a group of data in the the east Labrador Sea in the long winter having relatively low heat content.

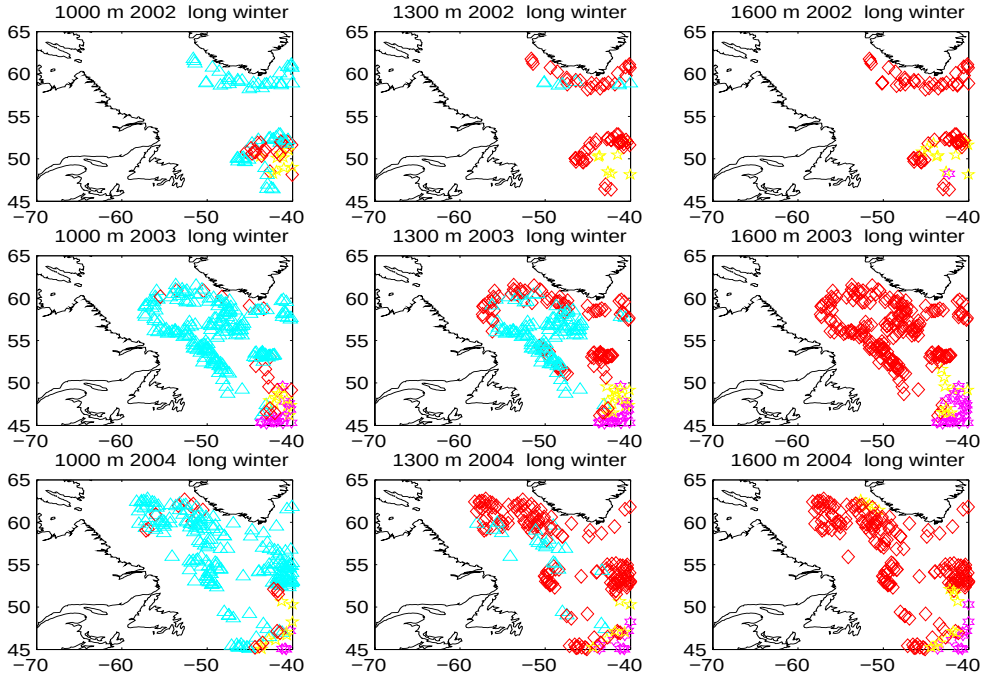

Figure 2.19. The heat content, HC above 1000 m, 1300 m, and 1600 m in the long winter (November -May winter). $0 < HC \leq 1 \times 10^{10}$ Jm^{-2} is marked with blue squares, $1 \times 10^{10} < HC \leq 2 \times 10^{10}$ Jm^{-2} with light blue triangles, $2 \times 10^{10} < HC \leq 3 \times 10^{10}$ Jm^{-2} with red diamonds, $3 \times 10^{10} < HC \leq 4 \times 10^{10}$ Jm^{-2} with yellow pentagons, and $HC > 4 \times 10^{10}$ Jm^{-2} with purple hexagons

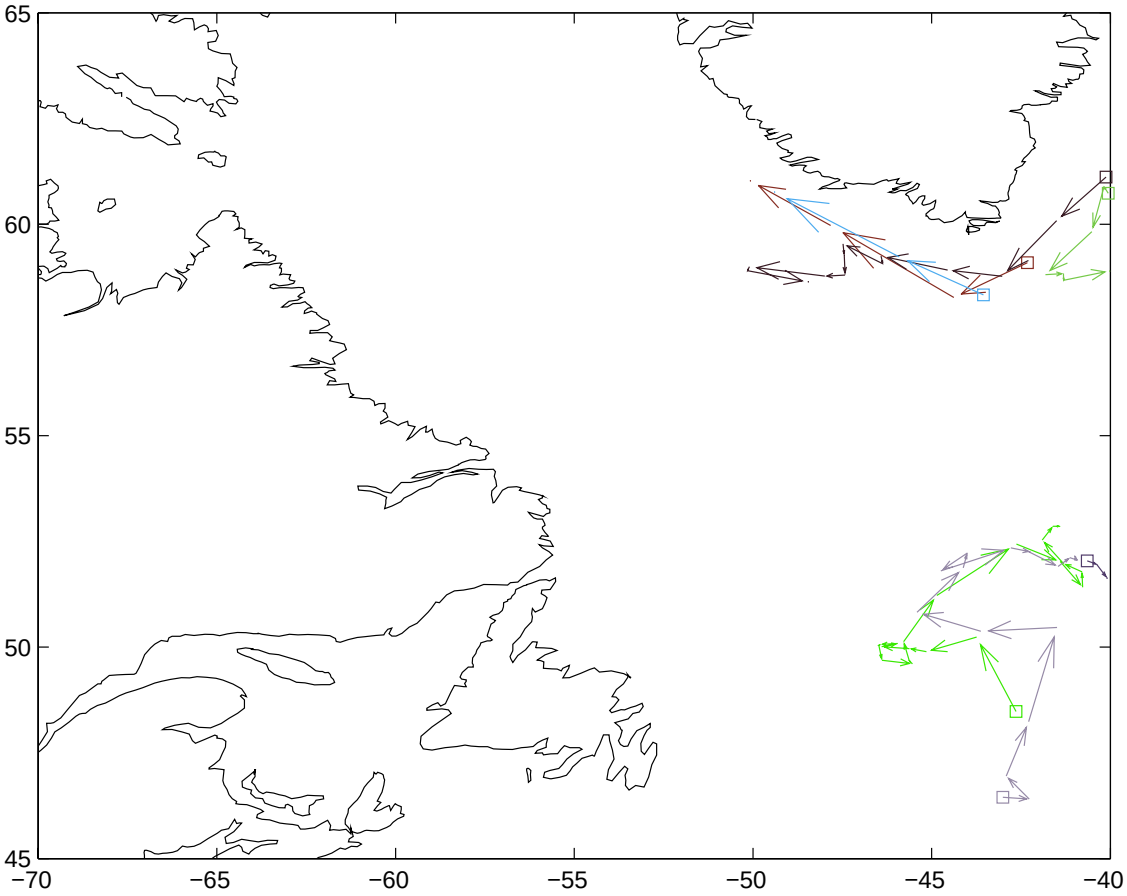

Figure 2.20. Trajectories of 7 floats at 2000 m in 2002 long (November-May) winter, squares denote the deployment locations of the floats

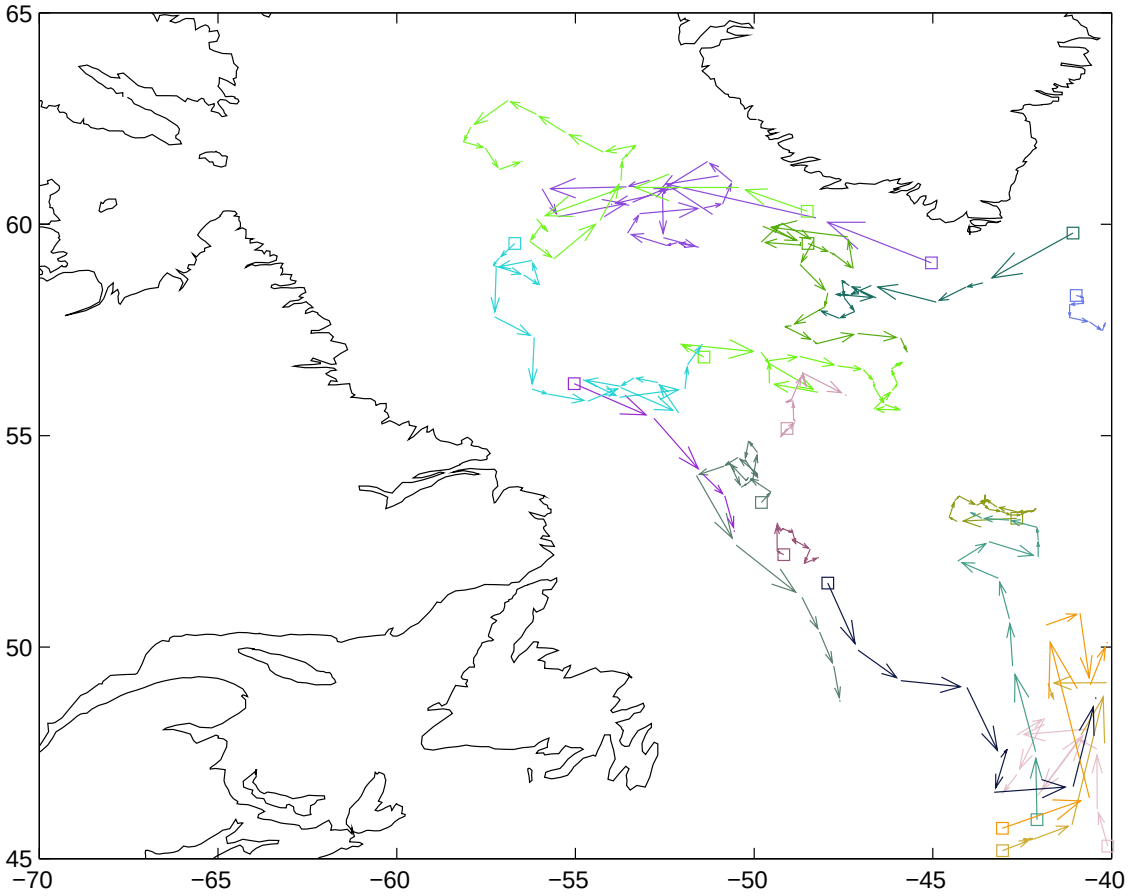

Figure 2.21. Trajectories of 19 floats at 2000 m in 2003 long (November-May) winter, squares denote the deployment locations of the floats

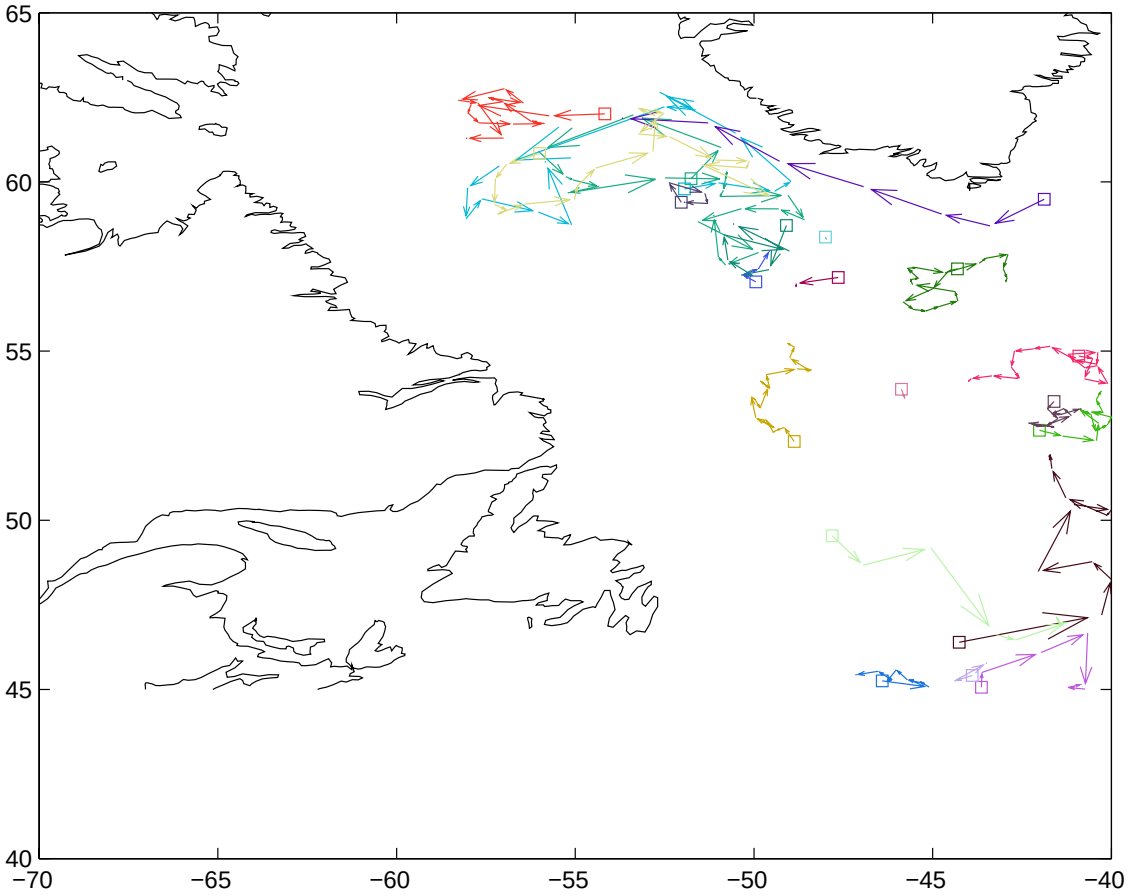

Figure 2.22. Trajectories of 23 floats at 2000 m in 2004 long (November-May) winter, squares denote the deployment locations of the floats

2.5 Trajectories of the floats at 2000 m

Figure 2.21 shows nineteen float paths and there are three important points we found: (1) Two circulating paths are found around 60^oN 54^oW and one is found around 59^oN 48^oW. These recirculations occurred at approximately the same locations as the recirculation observed by Lavender *et al.* (2000) at 700 m. This suggests that recirculation still exist at 2000 m. (2) A 'sub-gyre' is observed around 56^oN in year 2003. (3) A well defined DWBC is presented from 56^oN down to 48^oN and also a branch of it (the black path of figure 2.21) flows southeastward to the NAC region. For 2004, around 60^oN 54^oW , there are more recirculation patterns.

2.6 Energy

To get a better understanding of the dynamics of the Labrador Sea at 2000 m, the mean kinetic energy (MKE) and the eddy kinetic energy (EKE) are calculated in 2×2 degree boxes for each year's long (Nov-May) winter. The former one quantifies the mean motion of the current, while the latter one quantifies the fluctuating motion of the current.

MKE and EKE are calculated by the following equations:

$$MKE = \frac{1}{2}\left(\overline{u}^2 + \overline{v}^2\right) \tag{2.3}$$

$$EKE = \frac{1}{2}\left(\overline{u'^2} + \overline{v'^2}\right),\ u' = u - \overline{u}, v' = v - \overline{v} \tag{2.4}$$

From 2.23, there are two common points among the three years' winter: (1) The scale of the MKE is approximate five times of that of the EKE. (2) There are always relatively high EKE near Cape Desolation of Greenland for each winter. This basically agrees with Eden and Boning (2002), who found high EKE on about the same region of the upper ocean and they also suggested the main EKE source for Labrador Sea is generated by WGC there.

For the 2002 and 2004 winters, the highest MKE are found around the NAC regions, this implies there would be relatively stable flow of water current. While in 2003, the high MKE are found close to the Deep Western Boundary Current (around 50^oN). Both in 2003 and 2004, the highest EKE is found on the west coast of Greenland. For 2003, this high EKE might bring the warmer Irminger Sea Water (ISW) into

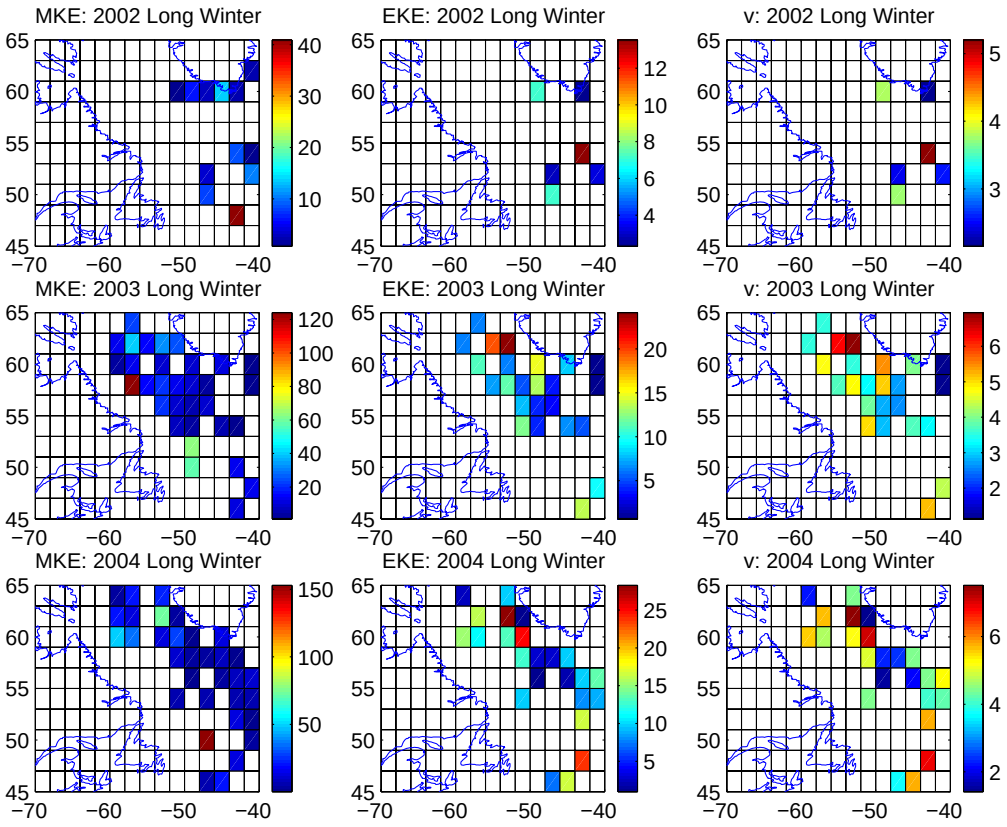

Figure 2.23. MKE, EKE, velocity derived from EKE for 2002-2004 long winters. The unit of MKE and EKE is cm^2s^{-2}, and the unit of velocity, v is cms^{-1}

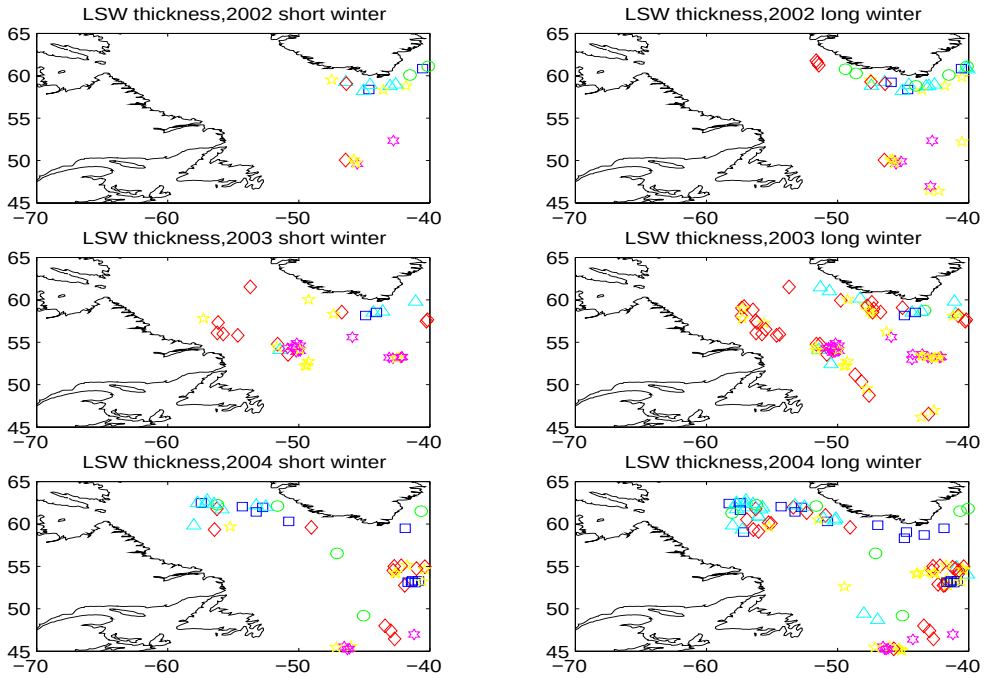

Figure 2.24. The thickness of the Labrador Sea Water, t is shown. $t \leq 600$ m is marked with green circles, $600 < t \leq 700$ m with blue squares, $700 < t \leq 800$ m with light blue triangles, $800 < t \leq 900$ m with red diamonds, $900 < t \leq 1000$ m with yellow pentagons, and $t > 1000$ m with purple hexagons

the interior Labrador Sea to enhance the deep convection, which is also suggested by Katsman *et al.* (2004).

We also derive the circulation velocity from the EKE by kinetic energy equation $KE = \frac{1}{2}mv^2$.

2.7 LSW thickness and the depth of potential vorticity

The thickness of the LSW is determined by the isopycnals ranging from 27.74 to 27.8 kgm^{-3}. Consistent with the distribution of the MLD, 2003 have highest number of thick LSW. On the other hand, the thickness is usually high around 55^oN among the three winters especially in 2003 long(Nov-May) winter. This is because the convection usually happens over there and is consistent with Stramma *et al.* (2004)'s work. The thick LSW layer found in the eastern Labrador Sea confirmed that LSW is spreading eastward or is due to the spreading of LSW from the Irminger Sea (Pickart *et al.* 2003).

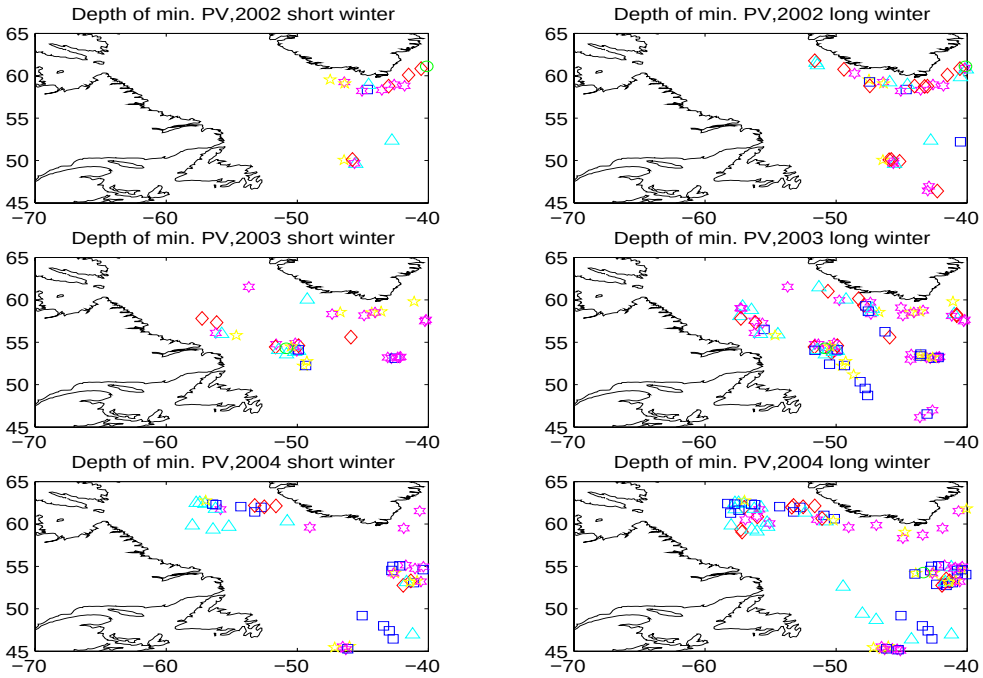

Figure 2.25. The depth of the potential vorticity minimum , d is shown. $d \leq 500$ m is marked with green circles, $500 < d \leq 750$ m with blue squares, $750 < d \leq 1000$ m with light blue triangles, $1000 < d \leq 1250$ m with red diamonds, $1250 < d \leq 1500$ m with yellow pentagons, and $d > 1500$ m with purple hexagons

The potential vorticity (PV) of baroclinic flow is given by:

$$PV = \frac{f}{\rho_o} \frac{\partial \rho}{\partial z} \tag{2.5}$$

which can be written as

$$PV = \frac{f}{\rho_o} \frac{\rho(z + \Delta z) - \rho(z)}{\Delta z} \tag{2.6}$$

by finite differences.
f is the Coriolis parameter, which is equal to $2 \times \Omega \times \sin \phi$, where Ω is the angular velocity of the earth(7.29×10^{-5} rads $^{-1}$) and ϕ is the latitude. ρ and z are the potential density and depth respectively. ρ_o is the reference potential density, which is taken as 1027.1 kgm^{-3}.

The depth of minimum potential vorticity indicated the position of the core of LSW. (Talley and McCartney 1982). On the other hand, it can reflect the position(ie.

depth) of the homogeneous water mass present. Figure 2.25 shows that the majority of the minimum PV depth exceeds 1500 m and they are mainly found along the coast of Greeland for the three years. This suggests that a homogenous water mass can be found over there under 1500 m. Actually, some of the deep MLDs are found also along the coast of Greenland and therefore the homogenous water mass with minimum PV may be the product of the deep convection over there.

3 Ocean Modelling

3.1 Sub-polar Ocean Model

The Sub-polar Ocean Model (SPOM) is a regional configuration of MOM-A(Modular Ocean Model-Array) designed to focus on the sub-polar North Atlantic region, and is a derivative of the OCCAM model run by the Southampton Oceanography Centre. MOM-A originates from the Bryan-Cox-Semtner model(1965-1989) developed in Geophysical Fluid Dynamics Laboratory (GFDL) of National Oceanic and Atmospheric Adminstration (NOAA). Among the difference between MOMA and GFDL's MOM is that the former is designed to be run on array processor computers. More background of MOM could be found in Haidvogel and Beckmann (1999).

The following table lists some important parameters and details of SPOM. The advantages and disadvantages of z-coordinate ocean models and grids B can be found in an article by Griffies *et al.* (2000), which details different kinds of ocean models.

Table 3.1. SPOM parameters and features

Parameter	value/discription
Resolution	$\frac{1}{3}^o$
Coordinate	z
Grid	B
Biharmonic horizontal viscosity coefficient, A_h	7.5×10^{18} cm^{4}s^{-1}
Diffusion coefficient,K_h	7.5×10^{18} cm^{4}s^{-1}
Vertical diffusion, K_v	0.3 cm^{2}s^{-1}
Momentum diffusion, A_v	1.5 cm^{2}s^{-1}
Time-stepping	60 s (barotropic part) 3600 s (baroclinic part)
Boundary	38^oN-70^oN, 0^oW-68^oW
Other features	flux-limited advection scheme, free surface, partial cell representation of bottom topography

SPOM is developed by Myers (2002*b*) and some of the major results and improvements seen with this model are summarised as following:

- SPOM reproduces the large scale gyre structure at the surface and major

elements of the hydrography, although with a common problem in eddy permitting ocean models: the deeper layers are too warm and salty.

- SPOM demonstrates anti-cyclonic counter currents, which are consistent with the observations by (Lavender *et al.* 2000).
- SPOM produces a good representation of the Labrador Current and the North Atlantic Current.
- LSW is formed convectively down to 1500 m offshore of the Labrador Current. Deep sinking is also found offshore of the West Greenland Current.
- A better choice of inflow conditions for the open southern boundary improved the representation of DWBC and the inflow of the Mediterranean Water.
- A Northern buffer zone improved the outflow from the Nordic Sea.
- A partial-cell scheme was used to represent the bottom topography, which improved the structure of the large scale gyre circulation, the total transports, the more dense water formation and distinct spreading pathways of LSW. More details about the impact of the partial cell scheme in SPOM can be found in Myers and Deacu (2004).

3.2 Model forcing fields

We use SPOM to simulate the sub-polar North Atlantic from 2002 - 2004, the same period we examined with the Argo data. The model is forced by wind stress and restoring boundary conditions, based on measurements of sea surface temperature (SST) and sea surface salinity (SSS). Both the SST and wind velocity are obtained from the NCEP-DOE Reanalysis 2 project run by the National Center for Environmental Protection (NCEP). This project uses a forecast system to perform data assimilation using past data from 1979-2001.

The wind velocity (u,v) is converted to wind stress by the following equation:

$$\tau_{\vec{u},\vec{v}} = \rho_a \, c_D \, V_{\vec{u},\vec{v}} \sqrt{\vec{u}^2 + \vec{v}^2} \tag{3.1}$$

where ρ_a is the density of air, set to 1.2 kgm^{-3}, c_D is a dimensionless drag coefficient which is equal to 0.0012, and $\vec{u}, \vec{v}$ are the components wind speed.

The SSS is the 40 years climatology which was used in previous simulation (Myers 2002*b*). The field was used because of the difficulty in obtaining sufficient interannual surface salinity data for the entire model domain.

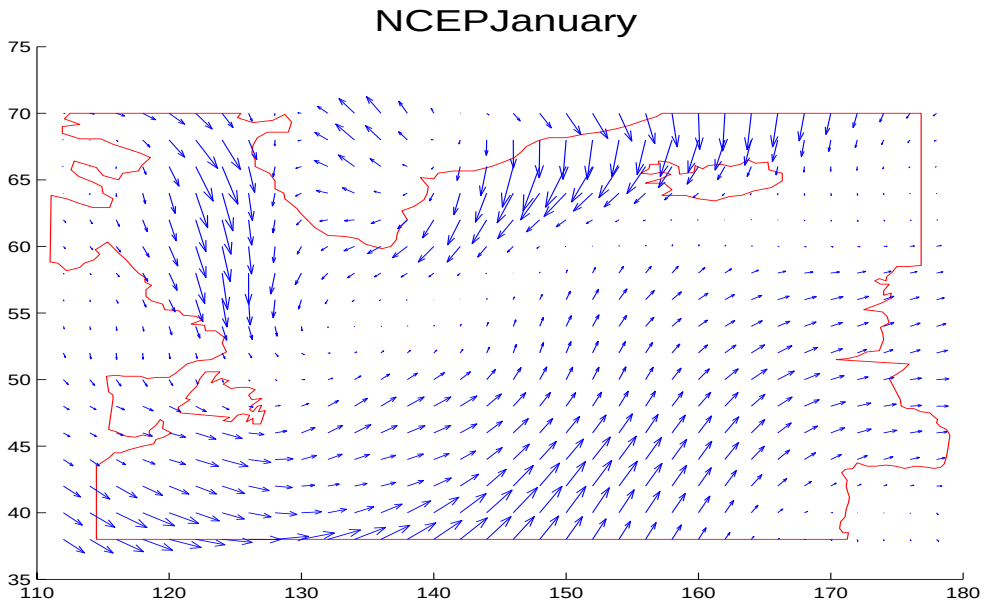

Figure 3.1. Monthly-averaged wind stress applied to the model for January

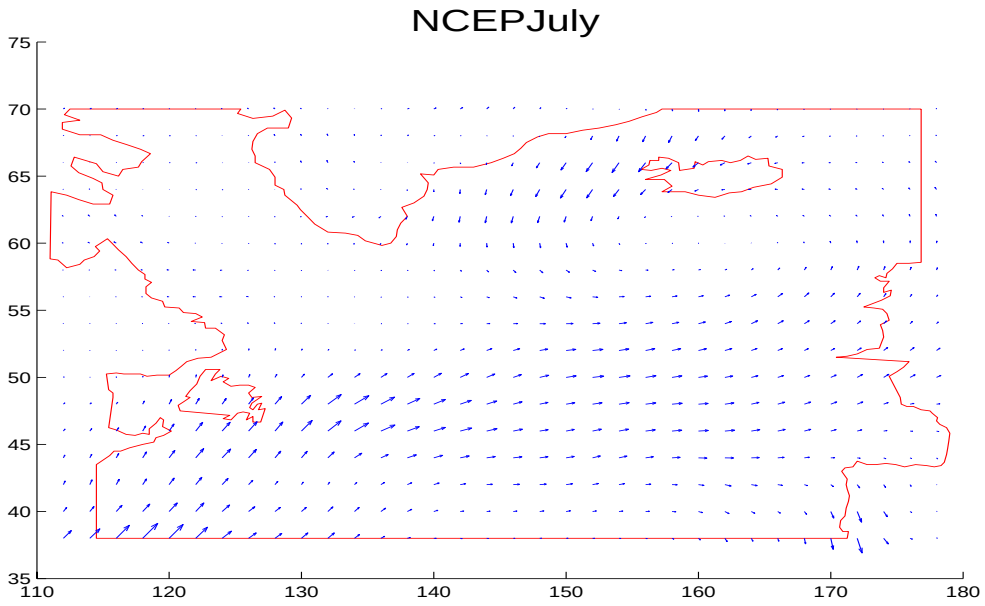

Figure 3.2. Monthly-averaged wind stress applied to the model for July

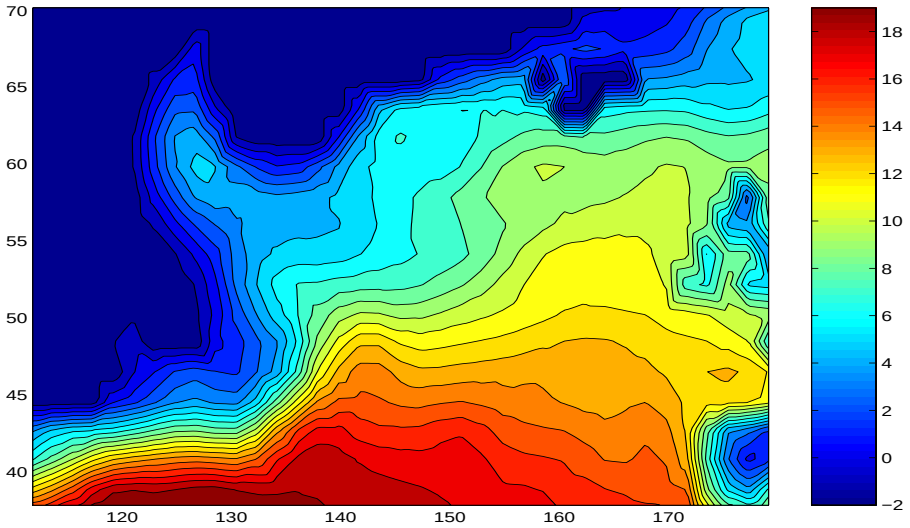

Figure 3.3. Sea surface temperature applied to the model for January

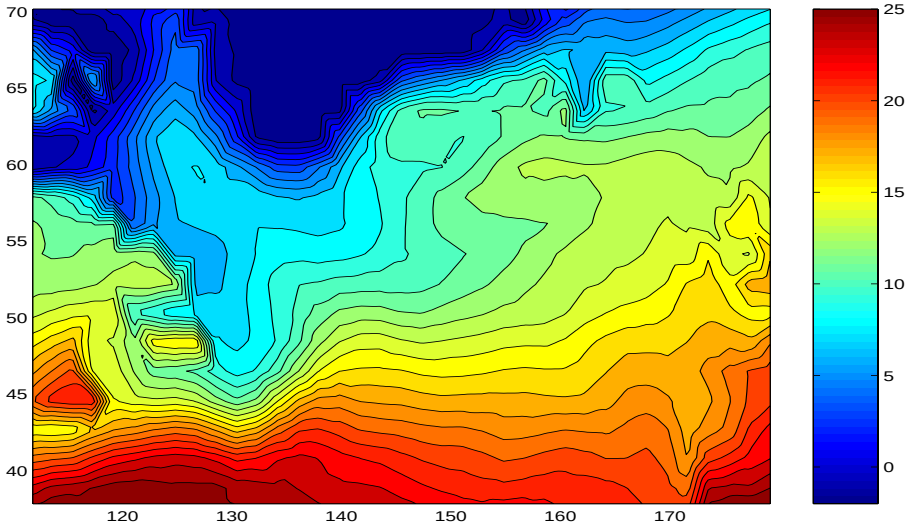

Figure 3.4. Sea surface temperature applied to the model for July

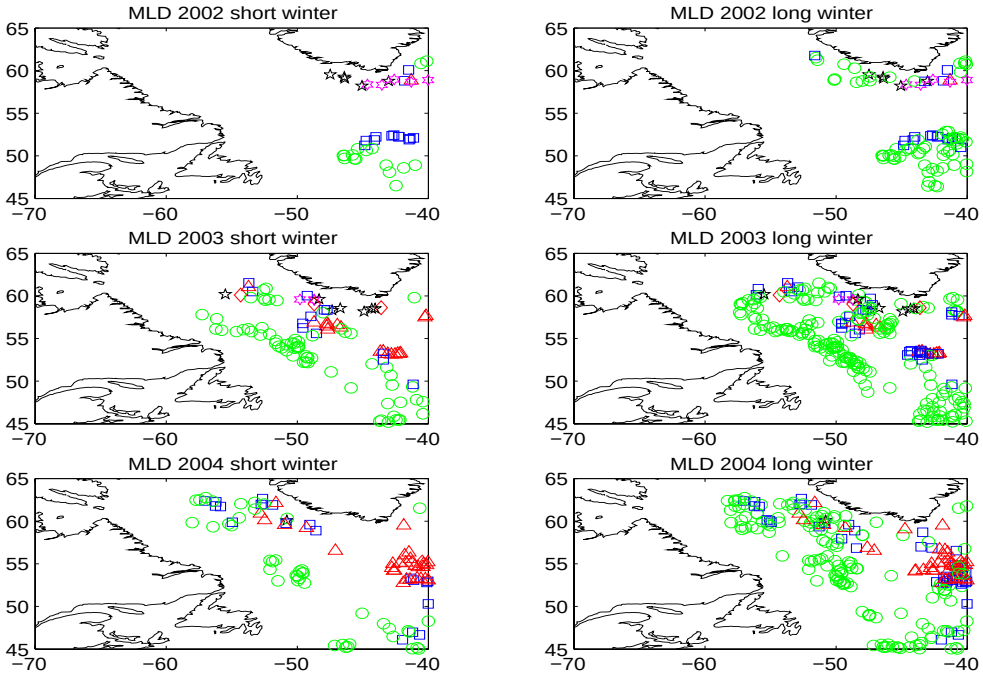

Figure 3.5. Model mixed layer depth, MLD. MLD $\leq$ 200 m is marked green circles, 200 $<$ MLD $\leq$ 500 m with blue squares, 500 $<$ MLD $\leq$ 800 m with light purple triangles, 800 m $<$ MLD $\leq$ 1100 m with red diamonds, 1100 m $<$ MLD $\leq$ 1600 m with black pentagons, and MLD $>$ 1600 m with purple hexagons

3.3 Model results

3.3.1 Mixed Layer Depth

Figure 3.5 shows the model MLD estimated on the corresponding locations of the float measurement from that winter. Generally, the model shows 2003 having the strongest deep convection. However, the deepest MLDs concentrate offshore the West Greenland Current region, not offshore the Labrador Current. The previous model result from the SPOM forced by 40 years of climatology also shows the deepest convection around the same region (Myers 2002*b*). For 2004, the location of deep convection is quite consistent with the observational results except a group of MLDs of 500-800 m that are found in the eastern Labrador Sea. Presumably, this might be attributing to the wind field of 2004, as Myers (2002*a*) did a experiment on the effects of different wind forcings on SPOM and found out that another wind sources, ECMWF (European Centre for Medium Range Weather Forecasts) gives a better performance for model simulations. This can be topic for a future work. For 2002, the location of model deepest MLD is about the same as the observational float results, though the model MLD is deeper. There are five points along the east coast of Greenland having MLD even greater than 1600 m. Basically, the model gives deeper MLDs than float data only in a few locations. This is due to the model's overestimation of salinity in the Labrador Sea. Generally, both the observational

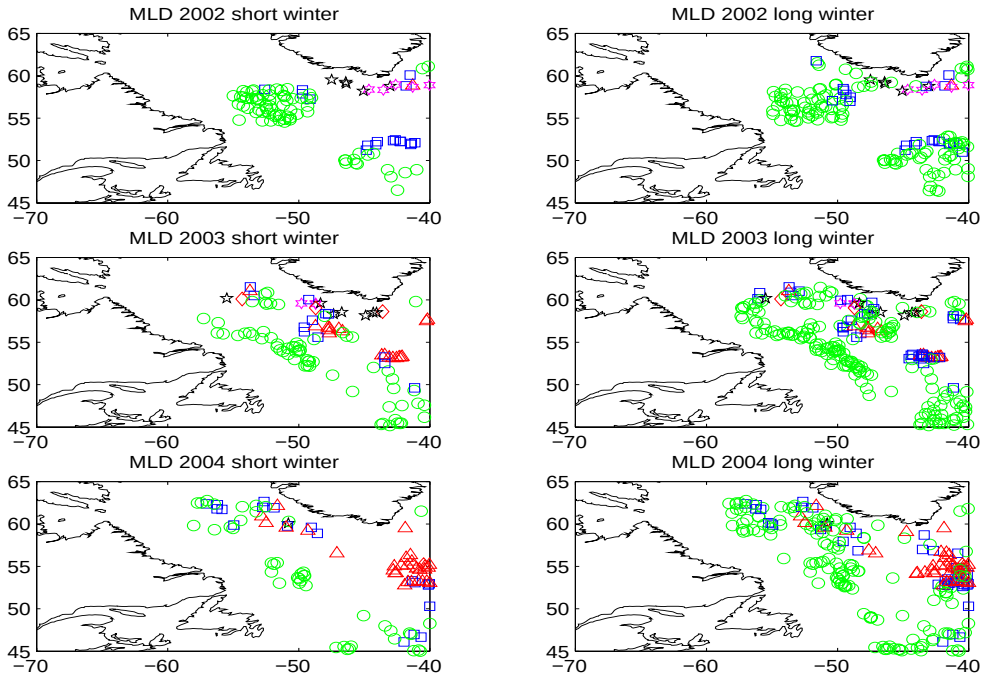

Figure 3.6. Model mixed layer depth with additional content in the central Labrador Sea in 2002, MLD. MLD $\leq$ 200 m is marked with green circles, 200 $<$ MLD $\leq$ 500 m with blue squares, 500 $<$ MLD $\leq$ 800 m with light purple triangles, 800 m $<$ MLD $\leq$ 1100 m with red diamonds, 1100 m $<$ MLD $\leq$ 1600 m with black pentagons, and MLD $>$ 1600 m with purple hexagons

and model results show similar intensity of deep convection (average $\sim$ 1100 m) on average.

Was the convection in 2002 stronger than that in 2003?

Referring to the the observational results in Chapter 2, we suspect 2002 might have the strongest deep convection and we now have three hypotheses: (1) $deep\,convection_{2002} > deep\,convection_{2003} > deep\,convection_{2004}$, (2)$deep\,convection_{2003} > deep\,convection_{2002} > deep\,convection_{2004}$ and (3) $deep\,convection_{2003} > deep\,convection_{2004} > deep\,convection_{2002}$. Figure 3.6 is the same as figure 3.5 except in the two winters of 2002, additional data are presented in the Labrador Sea to compensate for the lack of float measurements in that winter. Apparently, there is no deep convection simulated in the central and western Labrador Sea. It is also known that there is no simulated deep convection presented in the central and western Labrador Sea in any of the winters through three years. The model result also may suggest 2002 has stronger deep convection than 2004 as 2002's average is higher (consistent with the observational results). Therefore, we confirmed that 2003's deep convection is the strongest among the three years and we accept the second hypothesis to be true: $deep\,convection_{2003} > deep\,convection_{2002} > deep\,convection_{2004}$.

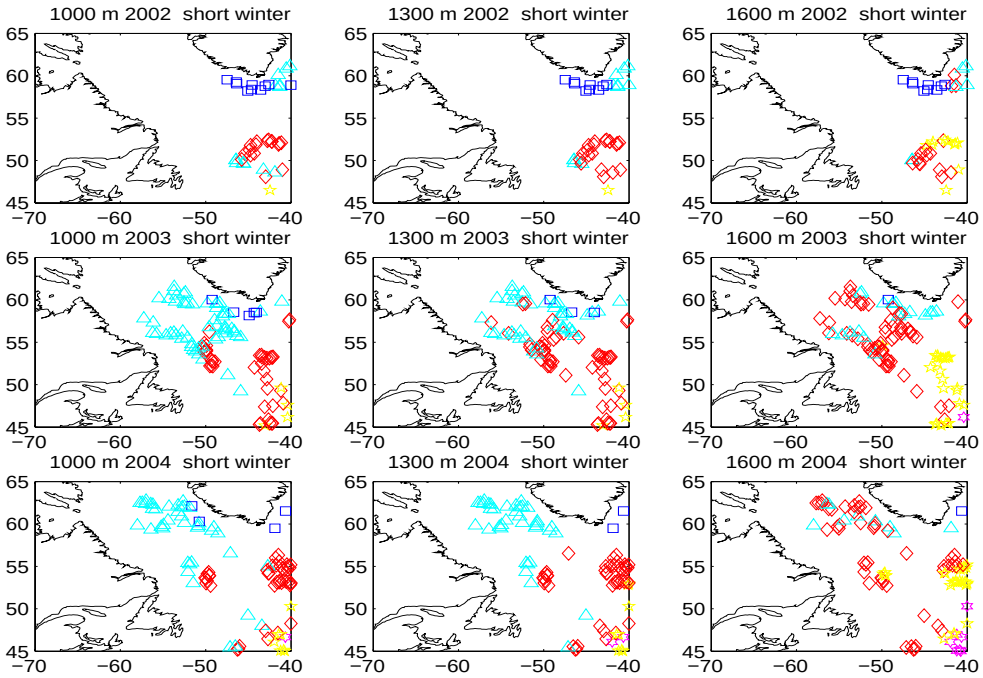

Figure 3.7. Model Heat Content in short (Jan-Mar) winter. $0 < HC \leq 1 \times 10^{10}$ Jm^{-2} is marked with blue squares, $1 \times 10^{10} < HC \leq 2 \times 10^{10}$ Jm^{-2} with light blue triangles, $2 \times 10^{10} < HC \leq 3 \times 10^{10}$ Jm^{-2} with red diamonds, $3 \times 10^{10} < HC \leq 4 \times 10^{10}$ Jm^{-2} with yellow pentagons, and $HC > 4 \times 10^{10}$ Jm^{-2} with purple hexagons

3.3.2 Heat content

The model shows results which are closer to the observational result of the short winters than that of long winters. This implies that the model is more 'realistic' from January to March. This may be related to the monthly average forcing of the model. The model always gives a lower heat content along the coast of Greenland than the observations, especially in 2002. In general, however, the model shows a relatively overall higher heat content than the observational results. In particular, the model gives high heat content of the eastern Labrador Sea region. This is because too much warm and salty North Atlantic Current water is entered into the model's Labrador Sea in the model.

3.3.3 Circulation

Figure 3.9, 3.10 and 3.11 show the monthly mean current at 1930 m over the long winter of each year. We do not see any remarkable difference between each plot,

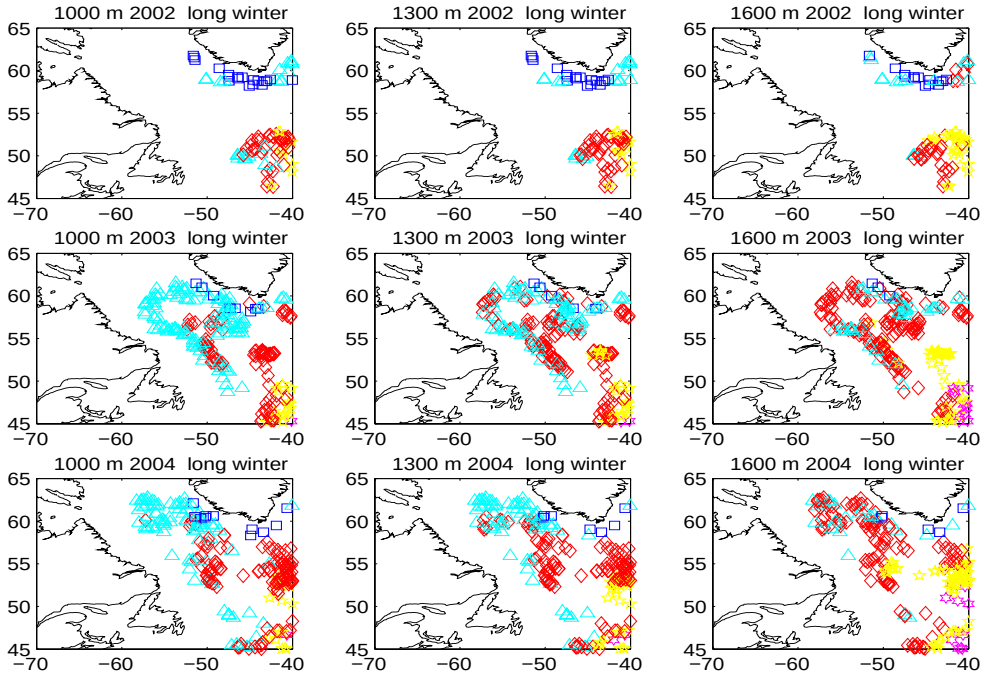

Figure 3.8. Model Heat Content in long (Nov-May) winter. $0 < HC \leq 1 \times 10^{10}$ Jm^{-2} is marked with blue squares, $1 \times 10^{10} < HC \leq 2 \times 10^{10}$ Jm^{-2} with light blue triangles, $2 \times 10^{10} < HC \leq 3 \times 10^{10}$ Jm^{-2} with red diamonds, $3 \times 10^{10} < HC \leq 4 \times 10^{10}$ Jm^{-2} with yellow pentagons, and $HC > 4 \times 10^{10}$ Jm^{-2} with purple hexagons

though we can still notice that the recirculation around 55^{o}N in 2002 is weakest among the three years. For 2004, there is an recirculation path from around 49^{o}N - 59^{o}N, which approximately corresponds to the two float paths (shown in brown in figure 2.21) from the observational results. At around 57^{o}N 51^{o}W, this model circulation also match well with the observational result. The model fails to depict the circulation at higher latitudes (around 62^{o}N), as the 2003 and 2004's observation show a distinct current pathway in this region.

In conclusion, the model circulation in all three years has the common characteristic of a distinct circulation path along the Greenland coast as well as a Deep Western Boundary Current offshore the Labrador shelf.

3.3.4 Energy

The MKE and EKE (figure 3.12) are computed in the same way as for the observational data, but are based on the velocity fields generated by the model at fixed grid points. This is different from the observation which is based on the float positions from each profile. The MKE, in general, is high along the coast of Greenland and the Labrador slope, as there are stable circulation paths in those regions (refer to

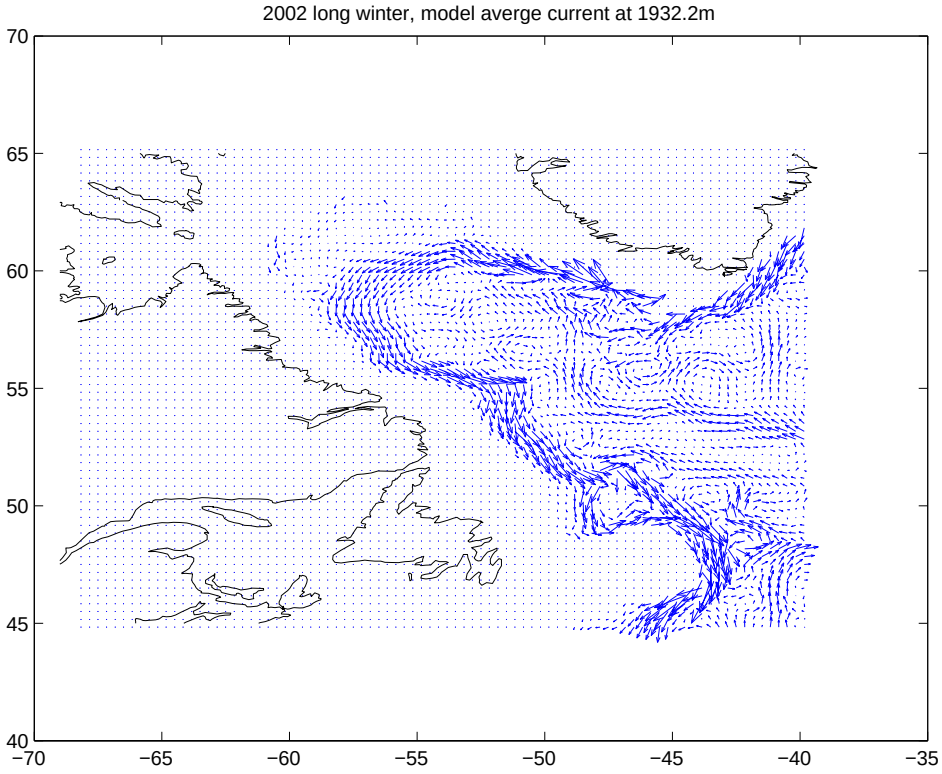

Figure 3.9. Average currents on the depth 1930 m during the 2002 long winter (22nd model level of Myers (2002b))

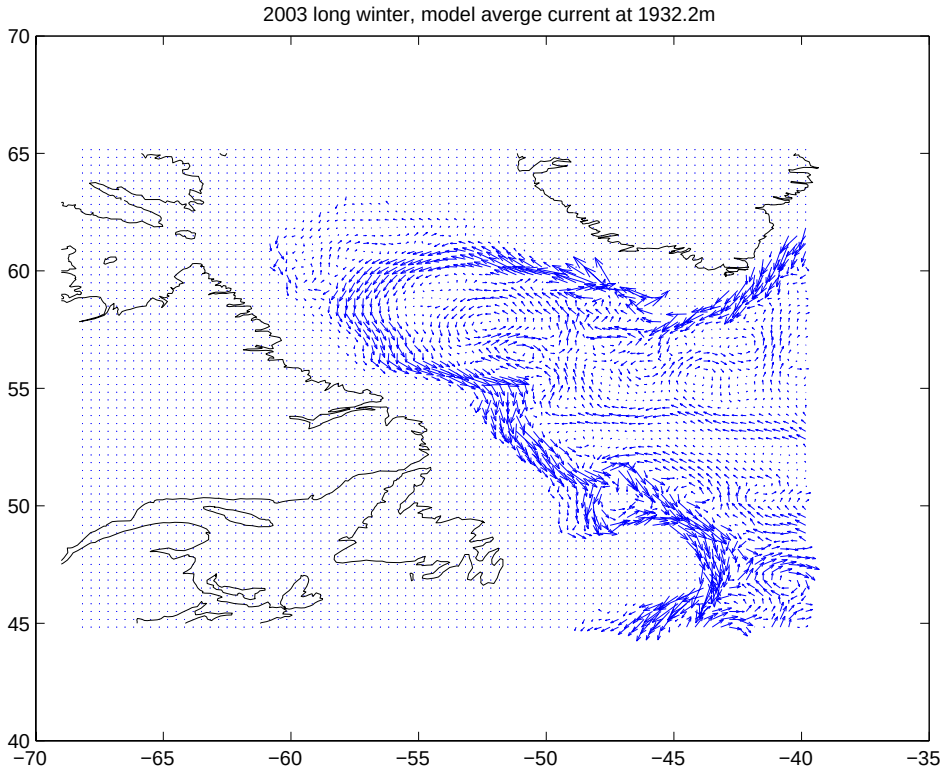

Figure 3.10. Average currents on the depth 1930 m during the 2003 long winter (22nd model level of Myers (2002b))

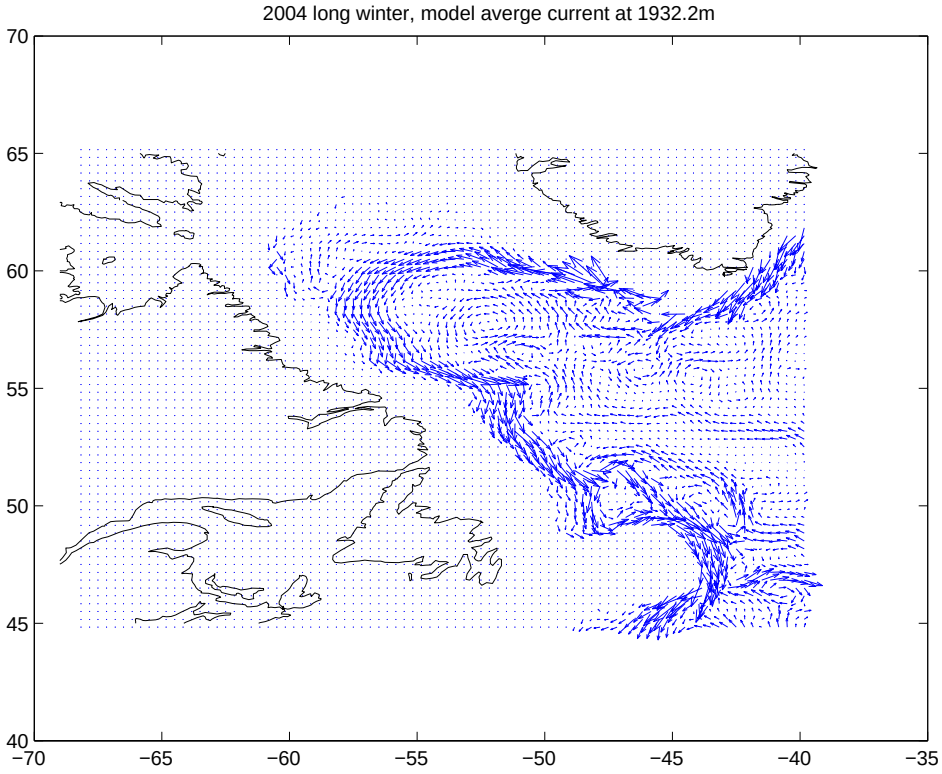

Figure 3.11. Average currents on the depth 1930 m during the 2004 long winter (22nd model level of Myers (2002b))

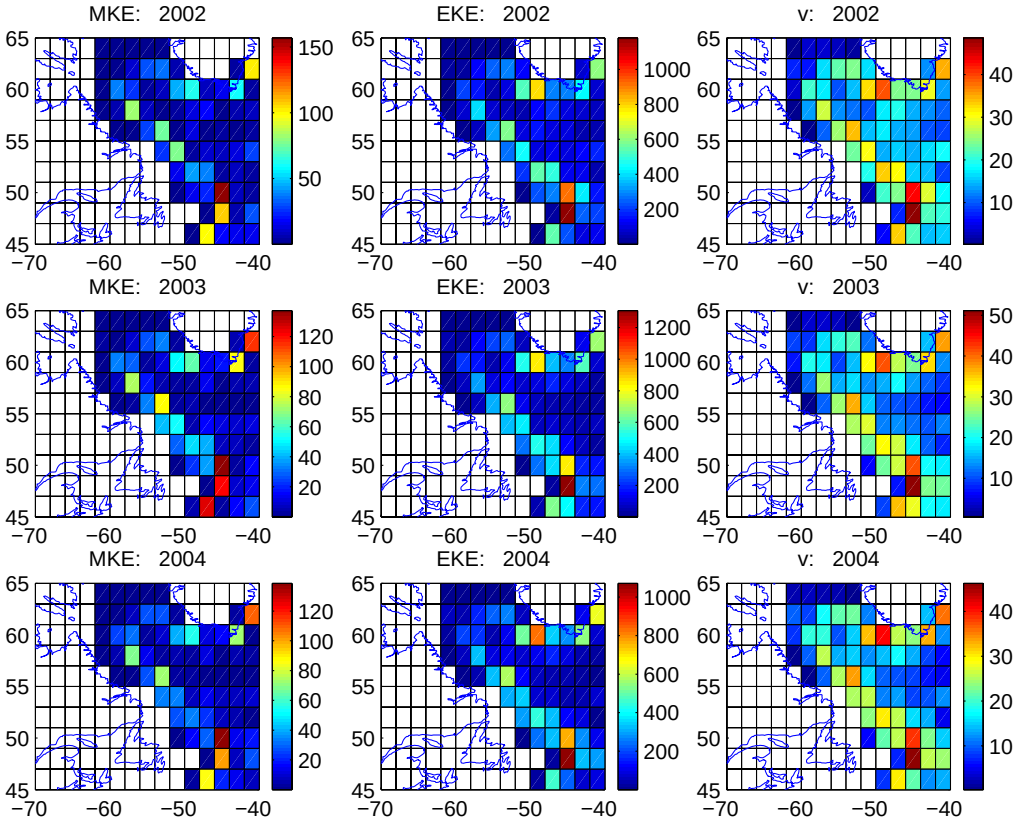

Figure 3.12. Model MKE, EKE, velocity derived from EKE for 2002-2004 long winters. The unit of MKE and EKE is cm^2s^{-2}, and the unit of velocity, v is cms^{-1}

3.9, 3.10, 3.11) and its magnitude is basically the same as the observational results in 2003 and 2004. But the highest MKE appears near the Flemish Cap and the North Atlantic Current accompanied by the highest EKE in all three years. The second highest EKEs are located offshore of the West Greenland Current, and agrees well with the observational result, as well as other studies, such as Eden and Boning (2002). This high EKE is important for building up the counter current and for exchange between the currents and the interior (Myers and Deacu 2004).

In spite of the magnitude of the model EKE is almost fifty times of the observational EKE, the distribution of the two EKEs is generally consistent except for a few locations. If we have higher resolution of floats, we might get higher EKE which might be comparable to the model EKE magnitude. This high model EKE is probably due to the strong currents caused by too warm and salty water in the bottom of the model.

4 Conclusion and Discussion

Both the Argo float result and the simulation result suggest that 2003 had the deepest convection (average $\sim$ 1100 m). Our overall result suggests that the deep mixed layers depth can be found beyond the traditional central or western Labrador Sea regions. Instead, deep MLDs could be found on the western coast of Greenland, Labrador slope and even in the NAC northwest corner region (with MLD 500 m - 800 m in year 2003). Whether these deep MLDs indicate local convective reoccurrence or thick layers of stratification is something that needs further study. Also in 2003, a clearly defined Deep Western Boundary Current (DWBC) is depicted in the trajectory. Throughout the investigation of the 2002 - 2004 winters, we found little or no obvious relationship and link between the inter-annual observation. This suggests the great variability of the Labrador Sea. Furthermore, the model results generally match well with the observational results, especially in some aspects such as high MLDs along the coast of Greenland and the DWBC.

Both Argo float measurement and modelling have their limitations. For Argo, there are coverage and accuracy limitations. In 2002, only about 40 % of the total number of floats collected proper profiles which could be used to estimate the MLD after the quality control, while for 2003 and 2004, there are about 75 % and 70 % of the total profiles usable to estimate the MLD respectively. We have also seen that just around 30 % of the total float profiles reach down to and drift at 2000 m in 2002, and approximately 70 % of that in 2003 and 2004. This might be due to the fact that it was just the beginning of Argo in the Labrador Sea. The year 2002 was the initial year of the Argo project and it took some time to get sufficient floats into the water. Additionally, a number of the early floats had technical problems. From these three years of data, we could see the availability of the profile has already been improved and remains steadily around 70 %. On the other hand, some of proper profile might be problematic because of sensor drift with Float 4900223 in 2004. It collected unexpected low salinity in the central Labrador Sea. After further examination, 4900223's profiles had to be omitted.

For the modelling, the NCEP wind and SST is monthly-averaged. However, in reality, wind is highly time dependent and can change abruptly within an hour while the the SST could also change within a day. SSS is the climatology of 40 years which cannot represent the ocean equilibrium state thoroughly. SPOM is a type of z model which has its own limitation, such as a rough representation of the bottom topography. All those factors can affect our model result significantly.

We have also other limitations, some of them are: the method we used to estimate the MLD is coarse especially in a weakly stratified region like the Labrador Sea; the density of the discrete data is low and linear interpolation is always employed.

Future work or the extension of this work could involve exploring the relationship between the North Atlantic Oscillation (NAO) index with the deep convection, the freshening sources of the North Atlantic, or improved models for sub-polar North Atlantic. But the biggest issue to consider from these preliminary result is how widespread the convection can be in the Labrador Sea (or beyond it, for example, in the Irminger Sea).

Bibliography

Bersch, M (1995). On the circulation of the northeastern North Atlantic. *Deep-Sea Research*, **42**, 1583–1607.

Clarke, R A and Gascard, J C (1983). The Formation of Labrador Sea Water. Part I:Large-Scale Processes. *Journal of Physical Oceanography*, **13**, 1764–1778.

Cuny, J, Rhines, P B, Niller, P P and Bacon, S (2001). Labrador Sea Boundary Currents and the Fate of the Irminger Sea Water. *Journal of Physical Oceanography*, **32**, 627–647.

Curry, R, Dickson, B and Yashayaev, I (2003). A change in the freshwater balance of the Atlantic Ocean over the past four decades. *Nature*, **426**, 826–829.

Davis, R E, Sherman, J T and Dufour, J (2001). Profiling ALACEs and Other Advances in Autonomous Subsurface Float. *Journal of Atmospheric and Oceanic Technology*, **18**, 982–993.

Dickson, B (1997). From the Labrador Sea to global change. *Nature*, **386**, 649–650.

Dickson, R, Curry, R and Yashayaev, I (2003). Recent changes in the North Atlantic. *The Royal Society*, **361**, 1917–1934.

Eden, C and Boning, C (2002). Sources of Eddy Kinetic Energy in the Labrador Sea. *Journal of Physical Oceanography*, **32**, 3346–3363.

Griffies, S M, Boning, C, Bryan, F O, Chassignet, E P, Gerdes, R, Hasumi, H, Hirst, A, Treguier, A and Webb, D (2000). Developments in ocean climate modelling. *Ocean Modelling*, **2**, 123–192.

Haidvogel, D B and Beckmann, A (1999). *Numerical Ocean Circulation Modeling*. Imperial College Press. London.

Hakkinen, S and Rhines, P B (2004). Decline of Subpolar North Atlantic Circulation During the 1990s. *Science*, **304**, 555–559.

Katsman, C A, Spall, M A and Pickart, R S (2004). Boundary Current Eddies and their role in the restratification of the Labrador Sea. *Journal of Physical Oceanography*, **34**, 1967–1983.

LabSeaGroup (1998). The Labrador Sea Deep Convection Experiment. *Bulletin of the American Meteorological Society*, **79**, 2033–2058.

Lavender, K L, Davis, R E and Owens, W B (2000). Mid-depth recirculation observed in the interior Labrador and Irminger seas by direct veloci ty measurements. *Nature*, **407**, 66–69.

Lavender, K L, Davis, R E and Owens, W B (2002). Observations of open-ocean deep convection in the Labrador Sea from subsurface floats. *Journal of Physical Oceanography*, **32**, 511–526.

Lazier, J, Hendry, R, Clarke, A, Yashayaev, I and Rhines, P (2002). Convection and restratification in the Labrador Sea, 1990-2000.. *Deep-Sea Research I*, **49**, 1819–1835.

Lazier, J R N and Wright, D G (1993). Annual Velocity variations in the Labrador Current. *Journal of Physical Oceanography*, **23**, 659–678.

Marshall, J and Schott, F (1999). Open-ocean convection: Observations, theory, and models.. *Rev. Geophys.*, **37**, 1–64.

Mizoguchi, K, Morey, S L, Zavala-Hidalgo, J, Suginohara, N, Hakkinen, S and OBrien, J J (2003). Convective activity in the Labrador Sea: Preconditioning associated with decadal varibility in subsurface ocean stratification. *Journal of Geophysical Research*, **108**, 28–1–28–10.

Myers, P G and Deacu, D (2004). Labrador Sea freshwater content in a model with a partial cell topographic representation. *Ocean Modelling*, **6**, 359–377.

Myers, Paul G (2002*a*). An examination of wind-stress forcing and circulation in the sub-polar North Atlantic. *Quaternary International*, **99-100**, 89–98.

Myers, Paul G (2002*b*). SPOM: A regional model of the sub-polar North Atlantic. *Atmosphere-Ocean*, **40**, 445–463.

Perez-Brunius, P, Rossey, T and Watts, D R (2004). Transformation of the Warm Waters of the North Atlantic from a Geostrophic Streamfunction Perspective. *Journal of Physical Oceanography*, **34**, 2238–2256.

Pickart, R S and Torres, D J (2001). Hydrography of the Labrador Sea during Active Convection. *Journal of Physical Oceanography*, **32**, 428–457.

Pickart, R S, Spall, M A, Ribergaard, M H, Moore, G W K and Milliff, R F (2003). Deep convection in the Irminger Sea forced by the Greenland tip jet. *Nature*, **424**, 152–156.

Rhein, M, Fischer, J, Smethie, W M, Smythe-Wright, D, Weiss, R F, Mertens, C, H, D, Fleischmann, U and Putzka, A (2000). Labrador Sea Water: Pathways, CFC Inventory, and Formation Rates. *Journal of Physical Oceanography*, **32**, 648–665.

Stramma, L, Kieke, D, Rhein, M, Schott, F, Yashayaev, I and Koltermann, K P (2004). Deep water changes at the western boundary of the subpolar North Atlantic during 1996 to 2001. *Deep-Sea Research I*, **51**, 1033–1056.

Straneo, F, Pickart, R S and Lavender, K (2003). Spreading of Labrador Sea Water: an advective-duffusive study based on Lagrangian data. *Deep-Sea Research I*, **50**, 701–719.

Talley, L D and McCartney, M S (1982). Distribution and Circulation of Labrador Sea Water. *Journal of Physical Oceanography*, **12**, 1189–1205.

Wilson, S (2000). Launching the Argo Armada Taking the ocean's pulse with 3,000 free-ranging floats. *Oceanus*, **42**, 17–19.

Woodgate, R, Fahrbach, E and Rohardt, G (1999). The structure and transport of the East Greenland Current at 75 n. *Journal of Geophysical Research*, **104**, 18059–18072.